# Hydrodeoxygenation of biomass-derived oxygenates over metal carbides: From model surfaces to powder catalysts



| | |
|---|---|
| Journal: | *Green Chemistry* |
| Manuscript ID | GC-CRV-01-2018-000239.R1 |
| Article Type: | Critical Review |
| Date Submitted by the Author: | 25-Apr-2018 |





| | |
|---|---|
| Complete List of Authors: | Lin, Zhexi; Columbia University, Chemical Engineering<br>Chen, Rui; Columbia University, Chemical Engineering; Nankai University, School of Materials Science and Engineering<br>Qu, Zhenping; Columbia University, Chemical Engineering; Dalian University of Technology, School of Environmental Sciences and Technology, Key Laboratory of Industrial Ecology and Environmental Engineering (MOE)<br>Chen, Jingguang; Columbia University, Chemical Engineering; Brookhaven National Laboratory, Chemistry Division |

# Hydrodeoxygenation of biomass-derived oxygenates over metal carbides: From model surfaces to powder catalysts

Zhexi Lin [a], Rui Chen [a,b], Zhenping Qu *[a,c] and Jingguang G. Chen *[a,d]

[a] *Department of Chemical Engineering, Columbia University, New York, NY 10027, USA*

[b] *School of Materials Science and Engineering, Nankai University, Tianjin, 300350, China*

[c] *Key Laboratory of Industrial Ecology and Environmental Engineering (MOE), School of Environmental Sciences and Technology, Dalian University of Technology, Linggong Road 2, Dalian, 116024, China.*

[d] *Chemistry Department, Brookhaven National Laboratory, Upton, NY 11973, USA.*

Corresponding authors: jgchen@columbia.edu (J.G. Chen); quzhenping@dlut.edu.cn (Z. Qu).

**Abstract**

The hydrodeoxygenation (HDO) reaction is critical to the upgrading of lignocellulosic biomass into valuable fuels and chemicals. Many transition metal carbide (TMC) catalysts have been shown to be highly selective toward the C-O/C=O bond scission, which makes them promising catalysts for the HDO reaction. This review summarizes the reaction pathways of linear and ring-containing biomass-derived oxygenates over TMC model surfaces and powder catalysts, followed by a discussion on the effect of reaction conditions on reaction pathways. The combination of first principle calculations, model surface experiments, and parallel reactor studies demonstrates the feasibility of using model surface science studies to guide the rational design of efficient catalysts for the upgrading of lignocellulosic biomass derivatives. General trends and future research directions of using TMC catalysts for HDO are also discussed.

## 1. Introduction

The catalytic upgrading of non-edible lignocellulosic biomass to fuels and chemicals is a promising way to mitigate the current environmental issues and to address the energy challenges. Various methods and processes have been developed to convert lignocellulosic biomass into cellulose, hemicellulose and then to C5 and C6 sugars, xylose, fructose and glucose.[1-5] These C5 and C6 sugars can then be converted into platform chemicals, including furfural and 5-hydroxylmethylfufural, which can be further upgraded to fuel additives such as 2-methylfuran (2-MF) or industrial-relevant chemicals such as p-xylene.[6]

One challenge for converting lignocellulosic biomass is that the biomass-derived molecules contain excess oxygen. The high O/C ratio limits the energy density of the biomass derivatives, as well as the selectivity to desired products during the upgrading processes.[7] In order to solve this problem, the excess oxygen needs to be removed via deoxygenation, which can be divided into two types of reactions: deocarbonylation/decarboxylation (DCO) and hydrodeoxygenation (HDO). The DCO reactions cleave the C-C bond associated with the carbonyl group or carboxyl group, resulting in loss of carbon and decreasing the energy content of the molecule. On the other hand, the HDO reaction selectively cleaves the C-O/C=O bond while preserving the carbon chain length. Moreover, under sufficient $H_2$ partial pressure, the HDO reaction removes oxygen in the form of $H_2O$ instead of $CO_2$ and is therefore more environmentally friendly than DCO regarding $CO_2$ emission.

Transition metal carbides (TMCs) have emerged as promising HDO catalysts. Molybdenum carbide ($Mo_2C$) and tungsten carbide (WC) have been shown to be highly selective toward C-O/C=O bond scissions. For example, Yu *et al.* have shown that $Mo_2C$ selectively cleaves the C-O bonds in ethylene glycol to produce ethylene, with the C-C bond remaining

intact.[8] Ren *et al.* have demonstrated that WC and $Mo_2C$ selectively cleave the C-O/C=O bond of C3 oxygenates, such as propanol and propanal, to produce propylene.[9,10] Ruddy *et al.* investigated the mechanism of the acetic acid HDO reaction and identified different types of active sites with different functionality.[11] Bhan *et al.* used the acetone HDO reaction to demonstrate the bifunctionality of $Mo_2C$ and the effect of oxygen modification on the active sites.[12] Additionally, there are a number of studies on the HDO of longer chain molecules, such as methyl stearate,[13-15] oleic acid,[16,17] stearic acid[13,18,19] and vegetable oils.[15,20-22] Model compounds for lignin derivatives, such as anisole[23-27] and guaiacol,[28-34] have also been thoroughly studied. Xiong *et al.* have reported that $Mo_2C$ is selective to the HDO of furfural to 2-methylfuran.[35] Several HDO reactions with $Mo_2C$ have been studied thoroughly using both experimental and computational approaches and detailed reaction mechanisms have been proposed.[9,10,36]

In additional to their high HDO selectivity, TMCs can be used as substrates to support metal catalysts for HDO reactions. Wan *et al.* have shown that the bimetallic Fe/Pt(111) surface is active toward the HDO reaction of furfural.[37] However, at elevated temperatures, Fe tends to diffuse into the Pt bulk, causing the HDO activity of Fe/Pt(111) to decrease. In contrast, by replacing the substrate from Pt(111) to $Mo_2C$, the stability of Fe/$Mo_2C$/Mo(110) is enhanced while maintaining similar HDO activity as that of Fe/Pt(111).[38] This is because the $Mo_2C$ substrate possesses Pt-like properties and can also serve as a barrier to prevent the Fe from diffusing into the bulk, therefore retaining the HDO activity with enhanced stability.[39-41] Similar enhanced stability is also observed on Co/$Mo_2C$/Mo(110) for the furfural HDO reaction, compared to Co/Pt(111).[42,37]

Research progress on the conversion of lignocellulosic biomass over TMC catalysts has been summarized by several reviews. Xiong *et al.* summarized and compared different bimetallic and TMC catalysts that can be used to achieve desired bond-cleavage sequence for reforming and HDO reactions of biomass-derived molecules.[7] Bhan *et al.* summarized the synthesis of TMCs and *in situ* chemical titration techniques to identify different sites on the bifunctional TMC catalysts.[43] Medlin *et al.* reviewed the bifunctional catalysts for the HDO reaction of pyrolysis oil and model compounds from biomass derivatives, with a focus on the influence of catalyst structures on reactivity.[44] This review aims to summarize the recent findings of HDO reactions of biomass-derived molecules with different structures (linear chain vs. ring-containing) over TMC model surfaces and powder catalysts. DFT calculations, surface science studies on single crystals, and reactor evaluations of powder catalysts are used as examples to demonstrate the feasibility of using results from well-characterized model surfaces to guide the rational catalyst design for upgrading biomass derivatives. General trends in the HDO of linear and ring-containing biomass-derived molecules over TMC surfaces are drawn, which are extended to reactor studies with the relevant TMC powder catalysts.

In this review, the HDO reactions over TMC catalysts are divided into two classes of biomass-derived oxygenates: linear chain and ring-containing molecules. The presence of the furan or benzene ring in a biomass-derived molecule can affect the HDO selectivity significantly. For example, due to the stabilization of the ring, it should be more difficult to cleave the carbon-oxygen bond in the furan ring of furfural than that in the carbonyl group. Sections 2 and 3 summarize and compare the reactivity of these two types of molecules over TMCs. The reaction conditions (temperature, pressure, etc.) play important roles in tuning the activity, selectivity and

stability of the TMC catalysts, which are reviewed in Section 4. Finally, general trends and opportunities in utilizing TMCs as HDO catalysts are discussed in Section 5.

## 2. HDO of linear chain oxygenates

Linear chain oxygenates represent an important class of biomass-derived molecules. Simple linear chain molecules are often used as model compounds for the study of more complex biomass derivatives. Their relatively simple molecular structures significantly reduce the computational expense, and their relatively high vapor pressures allow the dosing into ultrahigh vacuum (UHV) chamber for single crystal studies. C2 linear molecule such as ethylene glycol, glycolaldehyde and acetic acid are good model compounds because they have the same C/O ratio as C5 and C6 sugars and contain various functional groups. For the study of unsaturated fatty acids with relatively long chains, acrylic acid can serve as a model compound because it has a shorter chain that contains one C=C bond and one carboxylic acid functional group. In order to highlight the HDO reactions of linear oxygenates over TMC catalysts, this chapter uses the reactions of C2 (acetaldehyde, glycolaldehyde and acetic acid) and C3 oxygenates (propanal, propanol, 2-propanol and acrylic acid) on TMC surfaces and powder catalysts as examples to demonstrate the selective C-O/C=O bond cleavage capability of TMCs. The HDO reactions of other oxygenates with longer chains over powder catalysts are also briefly summarized. A list of linear chain oxygenates and the relevant techniques used for studying the HDO reactions on TMC catalysts can be found in Tables 1 and 2.

**Table 1**

## 2.1 Reactions on TMC surfaces

### 2.1.1 C=O/C-O bond scission of C2 oxygenates

As a major product of the *ex situ* catalytic fast pyrolysis (CFP) of biomass, acetic acid can be converted via various pathways, including DCO, HDO and ketonization (KET).[11] Acetic acid contains a C-O bond and a C=O bond. Therefore, it can be used to probe whether the carbide surface can promote the cleavage of one bond or both carbon-oxygen bonds. Using a combination of DFT and UHV techniques, Yu *et al.* demonstrated that acetic acid undergoes complete C-O/C=O bond scission to produce ethylene on the WC surface.[45] In comparison, when modified by Ni, the Ni/WC surface tends to break the C-C and C-H bonds to yield the reforming products ($CO + H_2$).

**Fig. 1**

**Fig. 2**

As shown in Fig. 1, TPD results reveal that ethylene is only produced on the WC surface, while $H_2$, CO and $CO_2$ are produced on the 0.5ML and 1ML Ni-modified WC surfaces. HREELS measurements (Fig. 2) demonstrate that acetic acid undergoes O-H scission to generate an acetate, $CH_3COO$, intermediate that binds to the WC and 1ML Ni/WC surfaces. The disappearance of the ν(C=O) mode (1711 $cm^{-1}$) at 200K indicates that the -COO group binds to the surfaces in a bidentate bonding configuration. The main difference between the WC and 1ML Ni/WC surfaces is that the C-C bond of acetate, indicative of the ν(CC) mode at 1028 $cm^{-1}$, is preserved on WC up to 600K but cleaved on 1ML Ni/WC at above 500K. This is consistent

with the ethylene peak temperature of 640K on WC, as well as production of $H_2$, CO and $CO_2$ between 500K and 600K on 1ML Ni/WC from the TPD results.

In order to compare the different interactions of the –COOH and –C=O functional groups on WC, TPD and HREELS measurements of acetaldehyde have also been performed on WC and Ni/WC surfaces.[45] the TPD results reveal that the primary products over WC is ethylene, which is formed by cleaving the C=O bond of acetaldehyde between 300K and 500K. On Ni/WC, the main products are $H_2$, CO and $CH_4$, indicating that acetaldehyde undergoes C-C and C-H scissions. HREELS experiments show that the ν(C=O) mode at 1650 $cm^{-1}$ of acetaldehyde is weakened upon increasing temperature to 200K and disappear at 300K, indicating that acetaldehyde changes to a di-σ bonding configuration at 300K. On Ni/WC, the attenuation of the δ(CCO) mode at 528 $cm^{-1}$ and the ν(CC) mode at 1109 $cm^{-1}$ at 300K suggests the start of C-C scission, which is consistent with the TPD results.

Vohs *et al.* performed surface studies on the reaction of glycolaldehyde over a $Mo_2C$ surface using TPD and HREELS.[57] It is demonstrated that below 550K, the primary product is ethylene, with ethanol and acetaldehyde as minor products. These three products are all produced from the deoxygenation reactions, indicating that $Mo_2C$ is highly selective toward the C-O/C=O scission. HREELS results reveal that at temperatures below 200K, glycolaldehyde bonds to $Mo_2C$ via an $\eta_1$(O) bonding configuration, which then transit to a di-σ $\eta_2$(C=O) bonding configuration between 200K and 300K. The di-σ $\eta_2$(C=O) configuration weakens the C=O bond, facilitating the subsequent C=O scission.[57]

**Scheme 1**

### 2.1.2 C=O/C-O bond scission of C3 oxygenates

The C3 oxygenates also represent a class of model compounds for studying more complex biomass-derived molecules. Similar to C2 oxygenates, C3 oxygenates undergo C-O/C=O scission selectively over TMC surfaces. Ren *et al.* studied the deoxygenation reaction of propanol and propanal over WC.[9] DFT calculations (Fig. 3) indicate that propanol and propanal undergo favorable C-O/C=O cleavages, with an activation barrier as low as 0.3 eV leading to the final product propylene. The DFT predicted reaction pathway is confirmed by TPD and HREELS experiments. From TPD experiments, for both propanol and propanal the main product on WC is propylene after selective C-O scission. HREELS results (Fig. 4) suggest that propanol undergoes O-H scission during the adsorption process to the surface due to the absence of the O-H stretching mode for propanol. On the other hand, propanal tends to bond to the surface via the di-σ bonding configuration, as evidenced by the disappearance of the C=O bond upon heating to 300K from 100K. Both propanol and propanal show a similar intermediate at 300K, consistent with the DFT calculations.

**Fig. 3**

**Fig. 4**

The HDO reactions of C3 oxygenates over $Mo_2C$ were reviewed previously.[7] Similar to WC, $Mo_2C$ shows high selectivity toward C-O/C=O bond scission. From DFT calculations, the probe molecule propanal preferentially undergoes C=O scission over $Mo_2C(0001)$ with an activation energy of 0.61 eV, rather than the C-C scission that requires 1.21 eV. Additionally, the relatively high activation barrier of the hydrogenation of propanal indicates that the C=O scission

happens in the absence of the initial hydrogenation step, and is also consistent with the major product being propylene instead of propane.

### 2.1.3 Summary of reactions of linear oxygenates over TMC surfaces

Scheme 2 summarizes the pathways of the C2 and C3 oxygenates discussed. Overall, from the studies of linear C2 and C3 oxygenates, $Mo_2C$ and WC have similar catalytic property at lower temperature (<550K). Both carbides tend to cleave all the C-O/C=O bonds to form ethylene or propylene as the major product. HREELS observations on the reactions of the C2 and C3 oxygenates suggest that in general WC and $Mo_2C$ interact strongly with the C-O/C=O bonds, which facilitates the cleavage of the bonds. It is also noticed that when WC is modified with Ni, the reaction pathway shifts from C-O/C=O scission toward the C-C bond scission.

**Scheme 2**

**Table 2**

**Table 3**

## 2.2 Reactor evaluations over powder TMC catalysts

### 2.2.1 HDO of C2 oxygenates

Schaidle *et al.*[11] evaluated and identified the active sites and HDO pathways of acetic acid over $Mo_2C$ with DFT calculations, *in situ* diffuse reflectance infrared Fourier transform

spectroscopy (DRIFTS) and X-ray photoelectron spectroscopy (XPS). HDO is the preferred pathway from 523 to 673K. This is generally consistent with the model surface results that $Mo_2C$ and WC surfaces selectively cleave the C-O/C=O bonds.

**Fig. 5**

The HDO reaction pathway over TMC catalysts also depends on the distribution of different types of active sites. Baddour *et al.* have studied acetic acid HDO over α-$MoC_{1-x}$ in SBA-15 silica [62] and identified two distinct sites on $Mo_2C$: acid site and H-site. The ratio of these two types of sites is the key factor for the HDO reaction, which can be influenced by the surface composition, crystal phase, and particle size. The $MoC_{1-x}$ nanoparticles with diameter of 1.9 ± 0.4 nm inside the pores of the support possess a greater acid-site/H-site ratio and exhibit a lower selectivity for HDO products and higher selectivity for DCO products, which is very different from bulk $Mo_2C$. The identity of different active sites and their influence on the catalyst performance will be further discussed in Section 4.2.

### 2.2.2 HDO of C3 oxygenates

Section 2.1.2 reviewed the DFT calculations and surface science experiments of C3 oxygenates over WC and $Mo_2C$. To bridge the pressure and material gap, Ren *et al.* also conducted reactor experiments to evaluate the HDO activity of powder WC and $Mo_2C$ catalysts.[9,10] On WC, propylene is the major product from both probe molecules, propanol and propanal. (Fig. 6) It is also observed that hydrogen partial pressure has different impact on

conversion. (Fig. 6) For propanol, co-feed hydrogen affects the conversion, while the effect for propanal co-feed hydrogen has less influence on the conversion.

**Fig. 6**

On $Mo_2C$, the DFT prediction and UHV results on model surfaces are verified by reactor evaluation (Fig. 7) with propanal, propanol, 2-propanol and acetone. Propylene is found to be the major product for all the reactants, with propane as the minor product. DFT calculations indicate that the activation barrier for the surface oxygen removal by hydrogen is significantly lower than that for the hydrogenation pathway to form propane. Therefore, hydrogen is mostly involved in the surface oxygen removal, and the selectivity to propane is low. Similar phenomenon was observed for acetic acid over $Mo_2C$.[11]

**Fig. 7**

Another important C3 oxygenates is acrylic acid. As the simplest organic acid containing one C=C bond and one carboxylic acid group, acrylic acid can be used as a model compound for studying unsaturated fatty acids. Recently Rocha *et al.*[61] investigated the HDO of acrylic acid on β-$Mo_2C/Al_2O_3$. Propane is found as the main product. DFT calculations reveal that acetic acid preferentially binds to the surface vis both the C=C double bond and the oxygen in the C=O bond. It is also found that the reaction proceeds through a hydrogenation/dehydration route where the cleavage of the C-O bond is favored over the C-C bond scission. The combination of DRIFTS, TPSR and DFT results identify an important intermediate $H_2C$=CH-CO, suggesting that unsaturated aldehydes could be an intermediate in the HDO of fatty acids over $Mo_2C$. This is

because the hydrogenation of the C=O bond has a much lower activation barrier (1.73 eV) than the C=C bond (3.47 eV), and is also more thermodynamically favored. A reaction network has been proposed (Fig. 8) for the HDO of acrylic acid on β-$Mo_2C/Al_2O_3$, where the carboxyl group of acrylic acid is hydrogenated instead of the double bond, producing an intermediate that leads to propane formation.

**Fig. 8**

One should also note that there is a trade-off for using simpler short chain molecules as surrogates. Smaller molecules often have higher vapor pressure and relatively simpler structures but could be significantly more reactive than the larger molecules that we are trying to predict. The selection of model compound is important. For example, the conjugation in short-chain surrogate molecule (e.g. acrylic acid) could influence the adsorption configuration compared to the longer chain molecules (e.g. oleic acid). Alternatively, 3-pentenoic acid should be a better model compound, since it is the simplest unsaturated acid that contains an internal C=C bond that is not conjugated to the -COOH group, and has a high enough vapor pressure for UHV studies.

### 2.2.3 HDO of other linear oxygenates over TMC catalysts

The HDO of vegetable oils composing primarily of triglycerides to alkanes is an important route to produce high-grade biofuels.[68] Oleic acid with one C=C bond and linoleic acid with two C=C bonds are abundant in the majority of vegetable oils.[69] Long chain oxygenates such as alkyl stearates, stearic and fatty acids and vegetable oils have also been studied for HDO over TMC catalysts. Although TMCs show promising HDO activity, the conversion of these

molecules into saturated hydrocarbons suitable for diesel fuel or linear olefins suitable for bulk chemical precursors require additional processing.[13-22,65,67]

Carbon materials, such as activated carbon (AC), carbon nanofibers (CNF), carbon nanotube (CNT) and mesoporous carbon (MC), are used as the supports because of their high surface area and electric conductivity that facilitate synthetic control over the TMC crystal phase and its dispersion. For example, $Mo_2C$/AC and $Mo_2C$/CNT show high activity in the HDO of vegetable oils and esters, such as bean oil, sunflower oil, maize oil, methyl stearate and methyl palmitate.[15,21,22] A high selectivity for branched hydrocarbons (85−95% of the total hydrocarbon yield) in a hydrogen-rich atmosphere ($H_2$/oil = 120−720 mole fraction) is obtained. Qin *et al.* have reported that $Mo_2C$/CNF is active for the HDO methyl palmitate to hydrocarbons.[20] $Mo_2C$ nanoparticles on the outside of the CNF show higher activity than the ones inside the CNF. $Mo_2C$/MC has been reported to show high HDO activity for the conversion of methyl stearate to octadecane with almost 100% conversion of methyl stearate and a high selectivity of 93.6% toward octadecane (T= 543 K, P=6 MPa).[14]

$Mo_2C$ catalysts supported on reduced graphene oxide (rGO), activated charcoal, graphite, and fullerene ($C_{60}$) have also been prepared and tested in the HDO of maize oil.[67] The activity order of the maize oil HDO reaction generally follows the trend of $Mo_2C$/rGO > $Mo_2C$/AC > $Mo_2C/C_{60}$, with $Mo_2C$/rGO showing a total hydrocarbon yield of 90.3% at 973 K. The uniform dispersion of the active $Mo_2C$ component on carbon supports is identified as one of the key factors for the catalytic activity.

Different deoxygenation pathways of carbide and oxide of tungsten have been reported in the reactions of stearic acid over CNF-supported $W_2C$ and $WO_3$ in a batch reactor.[13] A high selectivity of the unsaturated HDO product, octadecene, is observed over the $W_2C$/CNFs catalyst

pretreated at 1273 K (W-1000 in Fig. 9), whereas DCO products are dominant for the $WO_3$ catalyst.[13] Similar trends are also observed for the HDO of methyl stearate, tristearin and a mixture (5% tristearin, 20% stearic acid, 5% methyl stearate).

**Fig. 9**

Hollak *et al.* have reported different product selectivity for the HDO of oleic acid over $W_2C$/ CNF and $Mo_2C$/CNF at 623 K under 5 MPa $H_2$ pressure. $Mo_2C$/CNF is more selective toward the production of paraffins, while $W_2C$/CNF is more selective toward olefins.[16] In comparison to the lower selectivity to hydrogenated products from C3 molecules (e.g. propane from propanal,[10] ethane from acetic acid[11]), a higher selectivity to paraffin over $Mo_2C$ from oleic acid could be attributed to the substantially higher hydrogen partial pressure used (5 MPa vs. 0.1 MPa). Furthermore, $Mo_2C$/CNF shows higher activity and reaction stability in comparison with $W_2C$/CNF.

Supported $W_2C$/CNF and $Mo_2C$/CNF of different crystallite sizes have also been examined for the HDO of stearic acid to hydrocarbons.[18] The TMC particle size appears to affect for both HDO activity and stability. The catalyst stability of both catalysts is clearly improved when the active species are supported on CNF. In addition, it is found that supported $Mo_2C$ shows higher weight-based catalytic activity with the increase of particle size from 2 to 10 nm. The surface-specific activity (TOF) is estimated to be a factor of 10 higher for the larger $Mo_2C$ particles.

### 3. HDO of ring-containing oxygenates

The investigation of TMCs for HDO at low temperature and pressure has been extended to furanic oxygenates and lignin derivatives. Furanics are oxygenates containing furan rings. For

example, furfural and 5-hydroxymethylfurfural are two platform furanic molecules that can be further upgraded via HDO to valuable fuels and chemicals, such as 2-methylfuran, furfuryl alcohol, dimethylfuran and levulinic acid.[6, 70] The lignin fractions of lignocellulosic biomass are amorphous polymers consisting of phenolic compounds, making lignin derivatives as viable biomass sources to produce aromatic compounds via HDO. The HDO reactions of furan and benzene ring-containing oxygenates are summarized in Tables 3 and 4. The C-C bond hydrogenation or the undesired C-C bond cleavage by hydrogenolysis can occur concurrently with HDO reactions. Due to the strong C-O bond strength (422–468 kJ $mol^{-1}$), it is often difficult to selectively break the C-O bond while preserving the aromatic ring. High temperature (500–700 K) and pressure (1–30 MPa) are usually used to cleave the C-O bond in an aromatic molecule and mitigate coking.[23] Due to their preference toward C-O/C=O bond scission over C-C bond cleavage, TMC catalysts have been explored for the HDO of both furanics and lignin derivatives HDO reactions. This section uses furfural and guaiacol as examples of ring-containing molecules to demonstrate the high HDO selectivity of $Mo_2C$. The HDO reactions of other ring-containing molecules over TMC catalysts are also summarized.

**Table 4**

### 3.1 Reactions on TMC surfaces

#### 3.1.1 C=O/C-O bond scission of furfural over $Mo_2C$ surfaces

The hemicellulosic fragment of lignocellulosic biomass can be converted into a platform chemical known as furfural, which can be further upgraded via hydrogenation or HDO reactions

to valuable chemicals, such as furfuryl alcohol, tetrahydrofurfuryl alcohol and 2-methylfuran (2-MF). [6] The conversion of furfural to 2MF, which requires selective removal of the oxygen from the C=O bond outside the furan ring, is of particular interest for fuel production (Scheme 3).

**Scheme 3**

Shi *et al.* performed detailed DFT and microkinetic calculations to provide fundamental understanding of the HDO reaction mechanism.[36] The DFT results provide insights into the adsorption configuration, activation barrier and the effect of hydrogen partial pressure on the product selectivity. As shown in Fig. 10, five adsorption configurations of furfural on a $Mo_2C(101)$ surfaces are compared, including the cis- and trans-furfural. The most stable configuration is the cis-furfural absorbed via the $\eta_2$(C=O) bonding configuration with the C=O bond elongated and furan ring tilted away from the surface (Table 5). Based on the optimized adsorption configuration, the subsequent activation barrier calculation on $Mo_2C(101)$ reveals that there is a critical initial step, in which the activation barriers of all possible pathways differ significantly. Two competing pathways are then identified: C-H scission to produce a F-CO intermediate that leads to furan formation and hydrogenation to produce a F-$CH_2O$ intermediate that results in 2-MF production.

**Fig. 10**

**Table 5**

The effect of hydrogen coverage on the reaction pathways has also been calculated on hydrogen pre-covered surface, as shown in Fig. 11. Compared to furfural on the clean $Mo_2C$ surface, the activation barrier for each pathway changes with the increase of hydrogen coverage. The furan production pathway is no longer favored. The two competing pathways become 2-MF production and furfuryl alcohol production, with F-$CH_2O$ being a common intermediate for both pathways. To bridge the pressure gap between first principle calculations and reactor studies, microkinetic modeling is performed to evaluate the activation barrier, reaction energy and reaction rate constant for the furfural HDO and DCO reactions over the $Mo_2C$ surface at reaction conditions (ambient pressure or $H_2$-pressurized condition). From Table 6, it is shown that DCO (furan production) is preferred on the clean $Mo_2C$ surface, while the HDO reaction (2-MF production) is preferred on 4H pre-covered surface, which is consistent with reactor study results that 2-MF production dominates at relatively high hydrogen partial pressure.[36]

**Fig. 11**

**Table 6**

The HDO of furfural over the $Mo_2C$ surface has been investigated using TPD and HREELS.[35,57,59] TPD results indicate that 2-MF is the major furan ring-containing product from furfural.[35] To determine if furfuryl alcohol is an intermediate for the conversion of furfural to 2-MF, Xiong *et al.* also performed parallel TPD and HREELS measurements following the reaction of furfuryl alcohol.[35] It is found that furfuryl alcohol also produces 2-MF with a similar

peak temperature as that of desorption of 2-MF produced from furfural. HREELS observations on furfural over $Mo_2C$ suggest that furfural primarily bonds to $Mo_2C$ via the carbonyl group.[35,57] The binding configuration changes from $\eta_1$(O) to di-σ $\eta_2$(C,O) configuration upon increasing the temperature from below 200K to 300K.[57] As shown in Fig. 12, a 2-MF-like intermediate is observed when temperature is increased to 300K after dosing furfural or furfuryl alcohol onto hydrogen pre-covered $Mo_2C$ (110).[35] This also suggests that furfural may first undergo hydrogenation on the carbonyl group to form furfuryl alcohol and then proceeds to form 2-MF, consistent with the DFT calculation.[36] The selective carbonyl C=O scission suggests that the C=O bond outside the furan ring is more reactive than that in the furan ring. The general similarity among DFT calculations, UHV experiments and reactor studies suggests the feasibility of using model surface calculations and experiments to guide the rational design of powder catalysts.

**Fig. 12**

### 3.1.2 DFT calculations of guaiacol over TiC surface

Guaiacol contains both phenolic and methoxyl functional groups and is reported as one of the main products from lignin depolymerization.[28] The HDO of guaiacol can be used to evaluate the catalytic activity and selectivity for the conversion of depolymerized lignin streams. DFT calculations have been performed to investigate the HDO reaction of guaiacol over a range of transition metal ceramics, including carbides.[73] Shown in Fig. 13 is the guaiacol HDO reaction energy comparison among $TiO_2$, TiC, TiN, $TiS_2$ and TiP. The TiC surface first dissociate $H_2$ into atomic H, which is then added to guaiacol to assist the cleavage of the C-O bond between the

benzene ring and the methoxy group (Ph-$OCH_3$ bond). The C-O bond in the –$OCH_3$ group is also broken and hydrogen is added to form $CH_4$ and $H_2O$. This deoxygenation/hydrogenation step of the -O-$CH_3$ group is thermodynamically favored as the reaction energy difference is over 1eV. The resulting phenol-like intermediate subsequently undergoes C-O scission to form a benzene-like intermediate and atomic oxygen, which is then hydrogenated and desorbs as water. The benzene-like intermediate is further hydrogenated and desorb as benzene. It should be noted that in this HDO pathway, the Ph-$OCH_3$ bond scission is preferred over the Ph-OH bond cleavage.

**Fig. 13**

**Table 7**

**Table 8**

### 3.2 Reactor evaluation over powder TMC catalysts

#### 3.2.1 Furfural HDO over $Mo_2C$

Bhan and co-workers[75] have reported that vapor phase furfural selectively undergoes HDO reaction to form 2-MF over $Mo_2C$ at low temperature (423K), with the C-C bond remaining intact. This is consistent with the DFT calculations and UHV studies that the $Mo_2C$ surface favors the carbonyl C=O scission to produce 2-MF over C-C scission to form furan.[35,36,57] A reaction mechanism has been proposed based on the surface studies by Madix *et al.*,[88,89] in which furfural adsorbs on the on-top site that is accountable for CO chemisorption, while atomic hydrogen adsorbs on a distinct site, likely a four-fold hollow site near the on-top

site. This agrees with the DFT models established by Shi *et al.*[36] Despite the high HDO selectivity, $Mo_2C$ is prone to deactivation caused by the decrease in the number of active sites. It is shown that increasing $H_2$ pressure helps slow down deactivation by preventing the oxidation of the carbidic sites.

### 3.2.2 Guaiacol HDO over $Mo_2C$ and $W_2C$

Several studies have been conducted for the HDO of guaiacol over $Mo_2C$ and $W_2C$ powder catalysts. It is generally agreed that guaiacol first undergoes demethoxylation to form phenol, which can be further converted to benzene via deoxygenation.[28-32] This is consistent with the DFT calculation that the Ph-OMe bond cleavage precedes Ph-OH cleavage described earlier (Section 3.1.2).[73] It is also proposed in some literature that catechol is an intermediate between guaiacol and phenol.[31] Comparing the Ph-OMe and PhO-Me bond, the former has a higher bond dissociation energy.[90] It is speculated that guaiacol should bind to $Mo_2C$ in a configuration that favors the cleavage of the more stable Ph-OMe bond instead of the PhO-Me bond.[77] It is also believed that the active sites for converting phenol to benzene can be poisoned by oxygen-containing molecules such as water.[84] Chang *et al.* have demonstrated that the conversion from guaiacol to phenol occur on the $MoO_x$ site present on the as-synthesized Mo/C catalysts, while the further Ph–O cleavage of phenol is catalyzed by the $Mo_2C$ site.[32] Another study by Roman-Leshkov *et al.* shows that $MoO_3$ is active and selective towards the HDO reaction of guaiacol to produce phenol, but higher temperature (>590K) is required.[90] To date, the adsorption configuration of guaiacol on TMC surfaces and the reaction intermediates involved in the HDO reaction are not yet well understood.

The effect of catalyst support on the HDO reaction of guaiacol over TMCs have also been investigated. Ordered mesoporous carbon (OMC) [21], CNT [22], CNF [16,20,28,30] and AC [31,32] have been used as supports for TMCs. Santillan-Jimenez *et al.* studied the HDO reaction of guaiacol over $Mo_2C$ supported on three types of carbon materials and found that the major products were phenol and catechol, with guaiacol showing 99% conversion and 49% yield to phenol over $Mo_2C$/CNF.[30] Jongerius *et al.* have reported the conversion of guaiacol into phenol and methylated phenols over a $Mo_2C$/CFN catalyst, with a total selectivity of 69% phenolics.[28] A comparison between different types of supported TMC catalysts shows that $W_2C$/CNF is also active, but not as active, selective and stable as $Mo_2C$/CNF. In addition, Li *et al.* have reported that guaiacol undergoes selective C-O bond scission to form mono-oxygenated phenols with a total selectivity of around 85% over the a-$MoC_{1-x}$/AC catalyst at 613K.[31] Li *et al.* have utilized sequential hydrothermal carbonization and temperature programmed reduction to synthesize core-shell graphite encapsulated $Mo_2C$ ($Mo_2C$@C) with promising activity, selectivity and stability. Guaiacol is selectively converted to phenol (68.6% selectivity) and phenolic compounds (93.5% selectivity) over $Mo_2C$@C with a conversion of 76.3% at 613K and 2.8 MPa.[29]

### 3.3 HDO of other lignin-derived oxygenates

As summarized in Table 4 TMC catalysts also show promising HDO activity for several other lignin-derived oxygenates, including anisole, m-cresol, phenol and vanillin. Anisole is often used as a surrogate for studying lignin derivatives since it contains a methoxy group, which usually exists in lignin-derived oxygenates. Bhan *et al.* have demonstrated the vapor phase anisole HDO reaction over $Mo_2C$ to produce benzene with over 90% selectivity between 420 K

and 520 K, which is significantly lower than the conventional reaction temperature. They also use *in situ* CO titration to show that metal-like sites participate in the HDO reaction.[23,24]

Lu *et al.*[25] have used a single-step carburization procedure to synthesize 3D-ordered mesoporous $Mo_2C$ and $W_2C$ with high surface area (>70 $m^2g^{-1}$) and turnover frequencies of around 9 and $2 \times 10^{-4}$ mol $mol_{CO}^{-1}$ $s^{-1}$ at ambient hydrogen pressure and 423−443 K. The ordered mesoporous $W_2C$ catalyst possesses the highest benzene selectivity in anisole HDO so far (> 96%), compared to other HDO catalysts such as transition metal phosphide ($Ni_2P/SiO_2$, $MoP/SiO_2$) (<20% benzene selectivity, 1.5 MPa of $H_2$, 573 K),[91] Pt–Sn bimetallic catalysts (<50% benzene selectivity, atmospheric pressure, 673 K),[92] $MoO_3$ (~56% benzene selectivity, 100 kPa of $H_2$, 593 K),[90] and $Mo_2C$ catalysts[23] (~90% benzene selectivity, 100 kPa of $H_2$, 423 K). Similar to the other studies on $Mo_2C$ and $W_2C$-based catalysts,[16,18,28] while $Mo_2C$ shows ~20% cyclohexane selectivity and ~80% benzene selectivity, $W_2C$ shows ~100% benzene selectivity, indicating that $W_2C$ favors the formation of unsaturated benzene over saturated cyclohexane. (Fig. 14)

**Fig. 14**

In order to study the HDO of pyrolysis vapor from lignin depolymerization, Chen *et al.*[77] use anisole, m-cresol, guaiacol and 1,2-dimethoxybenzene as model compounds, each of which contain a Ph-OH or Ph-$CH_3$ bond. Scheme 4 summarizes the reaction pathways of the phenolic oxygenates. Anisole, dimethoxybenzene and guaiacol all undergo Ph-O scission to form benzene as the final product, with anisole and phenol being intermediates for the HDO of dimethoxybenzene and guaiacol, respectively. As for m-cresol, the Ph-O bond is selectively

broken to form toluene as the final product, which is evidenced by the increase of toluene selectivity as the m-cresol content increases. The HDO of vanillin, a typical aldehyde product from the pyrolysis of lignin, has also been reported. The 20.0%$Mo_2C$/AC catalyst is highly active and stable for the HDO of vanillin, with a conversion of 93.2% and a p-cresol yield of 50.1% under mild conditions (1.0 MPa, 373K, 3h).[85]

Guo *et al.* used $W_2C$/AC to selectively catalyze C-O cleavage of several lignin model compounds.[81,82] The catalyst demonstrates good regenerability (5 times) and high yields to liquid oils (up to 70.7%) and C-O scission products (up to 96.8%) from lignin in methanol under a relatively low hydrogen pressure (0.69 MPa).[82] The high yield of aromatic liquid oil without any cycloalkane for $W_2C$/AC suggests that the catalyst is highly selective in activating the aryl ether bonds. The effect of the lignin structure from different plant botanical species (hardwood, softwood, and corn stalk) leads to different HDO activity of $W_2C$/AC for the production of aromatic chemicals, thus providing useful information on the yield and distribution of phenolic products with the structure of lignin.[81]

## 4. Effect of reaction conditions and catalyst stability

### 4.1 Effect of reaction temperature and hydrogen pressure on HDO activity

For the HDO reactions of biomass-derived molecules reviewed, the reaction conditions (temperature, pressure) play important roles in controlling the activity and selectivity of the TMC catalysts. It is important to optimize the reaction temperature for desired HDO products.

In addition to temperature, $H_2$ partial pressure also influence the reaction pathway significantly.

As shown in Section 3.1, higher hydrogen partial pressure can significantly promote the HDO reaction pathway over others. For example, 2-MF production is favored at relatively high hydrogen partial pressure, while furan production is favored at low hydrogen partial pressures.[36] Another example is the HDO of stearic acid, which shows nearly linear relationship between conversion and the initial hydrogen pressure between 0 and 1 MPa. As the initial hydrogen pressure reaches 1 MPa, stearic acid is fully converted. Increasing the hydrogen pressure from 1 MPa to 4 MPa greatly enhances the selectivity to n-octadecane while suppressing the reaction pathway to n-heptadecane formation.[19]

### 4.2 Effect of oxygen on HDO activity

The presence of surface oxygen on TMC catalysts affects the HDO activity. Hwu *et al.* have investigated the effect of oxygen modification on the C/W(111) surface for methanol decomposition and found that after oxygen modification, the selectivity to methane (C-O bond scission) is slightly reduced, while the CO selectivity (C-H and O-H bond cleavage) is enhanced.[58] Ren *et al.* have demonstrated that surface oxygen can poison the HDO active sites for propanol/propanal on $Mo_2C$, however, surface oxygen can be readily removed in the form of water by hydrogen, consistent with the relatively low activation barrier, predicted by DFT calculations.[10] Two types of active sites are identified for the HDO reaction of linear chain molecules over $Mo_2C$. One is the metal-like site for hydrogen dissociation, while the other is an acid site for the C-O cleavage.[11,12, 62] Ruddy *et al.* have also reported that the $Mo_2C$ surface is partially oxidized following pretreatment and exposure to reaction conditions and proposed an oxygen vacancy site, in addition to the metal-like and acid sites. Importantly, the cleavage of the

C=O bond of acetic acid takes place either over the acid sites of the partially oxygenated surface or over an oxygen vacancy at the surface of the oxycarbide species.[11]

The ratio of acid sites to metal-like sites can influence the HDO activity significantly and is dependent on the crystal phase, surface termination, composition and/or particle sizes.[62] *In situ* oxidation and extended reductive pretreatment can be used to tune the metallic−acidic bifunctionality of $Mo_2C$ to control the HDO reaction. Bhan and co-workers have used 13.5 kPa $O_2$ co-feed at 369 K to modify the $Mo_2C$ catalysts, resulting in a decrease of catalyst surface area from 68 to 9 $m^2$ $g^{-1}$ and an increase of Bronsted acidity. The metallic hydrogenation functionality and the HDO pathway via the carbonyl hydrogenation initial step are simultaneously suppressed due to the loss of C=O hydrogenation sites upon oxygen modification.[12] Sullivan *et al.* demonstrate that Brønsted acid sites are responsible for the dehydration of isopropanol to propylene at 415 K over $Mo_2C$ and that these sites evolved from the interaction of oxygen with the $Mo_2C$ surface (O*-$Mo_2C$).[65]

In the case of the HDO reaction for ring-containing molecules, two types of distinct sites are also identified, one of which is a metal-like site.[23,25,76] Bhan *et al.* show that the function and composition of the $Mo_2C$ catalyst can be modified by oxygen under reaction conditions.[76] Lee *et al.* report that the high deoxygenation selectivity (>90%) and low hydrogenation selectivity of anisole HDO over $Mo_2C$ can be ascribed to the O adsorption on $Mo_2C$ during reaction. The activity and selectivity of the $Mo_2C$ catalyst is significantly influenced by oxygen.[23] They also demonstrate that $Mo_2C$ undergoes inevitable oxidation before and during reaction. The metal-like sites necessary for HDO reaction are prone to be poisoned by surface oxygen. Bhan and coworkers [76] have systemically investigated the vapor-phase m-cresol HDO rates on oxygenate-modified $Mo_2C$ catalysts prepared by pretreating fresh $Mo_2C$ catalysts in 1 kPa of $O_2$, $H_2O$, and

$CO_2$ at 333 K. The results show that the metal-like sites needed for the HDO reaction are subject to poisoning by surface oxygen species and that fresh $Mo_2C$ is more likely to be poisoned by molecular oxygen. Compared with fresh $Mo_2C$, $Mo_2C$ modified by low concentration of oxygen reduces the production rate of benzene from anisole due to the poisoning of some of the active sites.[24]

### 4.3 Stability, deactivation and regeneration of TMC catalysts

Despite the promising selectivity toward C-O/C=O scission, TMC catalysts deactivate relatively easily. Understanding the deactivation of TMC catalysts during HDO reactions is of great importance for improving their catalytic performance. The deactivation of TMCs is mainly caused by oxidation, coke formation and particle growth. The deactivation of TMCs in the presence of water has been reported and associated with the formation of $MoO_2$ and oxycarbides.[25,75,79,93] Lee *et al.* demonstrate the *in situ* formation of oxycarbides that deactivate $Mo_2C$ toward the furfural HDO reaction.[75] $Mo_2C$ also shows deactivation during the vapor-phase HDO of anisole.[25] Boullosa-Eiras *et al.* have also found that the HDO of phenol to form benzene is gradually decreasing with time over the $Mo_2C/TiO_2$ catalyst, whereas the selectivity to cyclohexene slightly increased, suggesting that the hydrogenolysis reaction is more prone to deactivation than the hydrogenation reaction.[78]

Despite the deactivation, it should be noted that TMC catalysts can often be regenerated. From Lu *et al.*, hydrogen treatment at 723K for 1 h effectively regenerates the deactivated $Mo_2C$ after anisole HDO. Moreover, the benzene synthesis rate of the regenerated $Mo_2C$ is about 30%

higher than that of the fresh catalyst.[25] This is possibly due to the recarburization of the catalyst surface during the $H_2$ treatment by the carbonaceous species left from the reaction. Similar phenomenon is observed from the HDO study of furfural over $Mo_2C$.[75]

## 5. Conclusions and future opportunities

This review summarizes the HDO reaction pathways of linear and ring-containing biomass derivatives over TMC model surfaces and powder catalysts. Due to their strong interaction with oxygen, TMC catalysts exhibit excellent C-O/C=O bond cleavage selectivity, which makes them promising catalysts for upgrading biomass-derived oxygenates. Several model compounds are used to illustrate the HDO activity over TMCs. In the case of C2 and C3 linear chain oxygenates, $Mo_2C$ and WC tend to cleave all the C-O/C=O bonds to produce ethylene and propylene, respectively. As for ring-containing molecules, the location of the oxygen significantly impacts the C-O/C=O bond reactivity. For example, the C=O bond in the carbonyl group in furfural is much more reactive than the C-O bond in the furan ring. Therefore, $Mo_2C$ selectively cleaves the carbonyl C=O bond to produce 2-MF. Despite their excellent C-O/C=O scission capability, TMCs are subject to deactivation due to the poisoning of oxygen and carbonaceous species, which interact strongly with the catalyst surface. In some cases, hydrogen is found to be capable of alleviating the deactivation by removing surface oxygen as water.

This review also demonstrates the feasibility of combining DFT calculations and microkinetic modeling with parallel experimental studies on model surfaces and powder catalysts to identify promising TMC catalysts for the HDO reaction of biomass derivatives. For instance, two competing reaction pathways of furfural over $Mo_2C$ (C-C scission and C=O scission) are identified by DFT calculation and microkinetics modeling. With the increase of

hydrogen partial pressure, the dominant pathway shifts from furan production (C-C scission) to 2-MF production (C=O scission), which is consistent with flow reactor results that higher hydrogen partial pressure promotes the C=O scission pathway to form 2-MF.

The summary of results in this review also points out several future research opportunities for upgrading biomass derivatives using TMC catalysts:

(1). Metal modifier can be deposited on TMC surfaces to lower the oxygen binding energy of TMCs to prevent or mitigate the deactivation due to oxygen poisoning. An approach similar to the design of bimetallic catalyst can be used. By choosing the correct metal modifiers, the surface d-band center of TMCs can be tuned to a proper extent such that oxygen should bind strongly enough to react and weakly enough to be removed from the surface to complete the catalytic cycle. *In situ* X-ray adsorption spectroscopy (XAS) techniques should also provide information on the metal termination, oxidation states and coordinate numbers to better understand the dynamics of the active sites of TMC and metal-modified TMC catalysts under reaction conditions.[94]

(2). The reaction mechanism and binding configuration of lignin derivatives over TMCs are relatively less understood. It is of importance to perform combined DFT calculations and single crystal studies to gain the mechanistic insights to guide the design of more efficient catalysts. One challenge is to identify proper model compounds that are small enough for DFT calculations of reaction networks, and have high enough vapor pressure to allow UHV studies on single crystal surfaces.

(3). As a by-product of biodiesel production, excess glycerol is available in large volume. The selective HDO reaction is an effective way of converting glycerol to more valuable compound, such as 1,3-propanediol and allyl alcohol. So far there are very few studies of

selective HDO of glycerol over TMCs. Due to the excellent C-O/C=O bond scission capability, TMCs and metal-modified TMCs are potentially good catalysts for the HDO reaction of glycerol.

(4). Recent studies have demonstrated the feasibility of electrochemical conversion of biomass derivatives.[95] TMCs and metal-modified TMCs have shown to be active and stable electrocatalysts for several electrochemical reduction and oxidation reactions.[96,97] It should be worth exploring whether these catalysts can be used for the electrochemical HDO reaction of biomass derivatives in both acid and alkaline electrolytes.

(5) Because the sulfide-form of Co/Mo/Ni catalysts are often used in the petrochemical industry for heteroatom removal,[98] it is also important to devote research effort to optimize the catalyst design and operation conditions. Multiple studies[99,100] have investigated the thermodynamics, kinetics and mass transfer of these sulfide-form catalysts, which should provide important information for further optimization for HDO reactions of biomass-derived oxygenates.

**Conflicts of interest**

There are no conflicts of interest to declare.

**Acknowledgements**

This article was sponsored by the Catalysis Center for Energy Innovation (CCEI), an Energy Frontier Research Center (EFRC) funded by the U.S. Department of Energy, Office of Basic Energy Sciences under Award Number DE-SC0001004. We thank Weiming Wan for the valuable discussion. We also acknowledge the VESTA visualization program,[101] which was used to prepare part of the table of content figure.

## References


1 J. N. Chheda, G. W. Huber and J. A. Dumesic, *Angew. Chemie - Int. Ed.*, 2007, **46**, 7164–7183.
2 G. W. Huber and A. Corma, *Angew. Chemie - Int. Ed.*, 2007, **46**, 7184–7201.
3 H. Wang, J. Male and Y. Wang, *ACS Catal.*, 2013, **3**, 1047–1070.
4 G. W. Huber, S. Iborra and A. Corma, *Chem. Rev.*, 2006, **106**, 4044–4098.
5 S. G. Wettstein, D. Martin Alonso, E. I. Gürbüz and J. A. Dumesic, *Curr. Opin. Chem. Eng.*, 2012, **1**, 218–224.
6 J. P. Lange, E. Van Der Heide, J. Van Buijtenen and R. Price, *ChemSusChem*, 2012, **5**, 150–166.
7 K. Xiong, W. Yu, D. G. Vlachos and J. G. Chen, *ChemCatChem*, 2015, **7**, 1402–1421.
8 W. Yu, M. Salciccioli, K. Xiong, M. A. Barteau, D. G. Vlachos and J. G. Chen, *ACS Catal.*, 2014, **4**, 1409–1418.
9 H. Ren, Y. Chen, Y. Huang, W. Deng, D. G. Vlachos and J. G. Chen, *Green Chem.*, 2014, **16**, 761–769.
10 H. Ren, W. Yu, M. Salciccioli, Y. Chen, Y. Huang, K. Xiong, D. G. Vlachos and J. G. Chen, *ChemSusChem*, 2013, **6**, 798–801.
11 J. A. Schaidle, J. Blackburn, C. A. Farberow, C. Nash, K. X. Steirer, J. Clark, D. J. Robichaud and D. A. Ruddy, *ACS Catal.*, 2016, **6**, 1181–1197.
12 M. M. Sullivan and A. Bhan, *ACS Catal.*, 2016, **6**, 1145–1152.
13 R. W. Gosselink, D. R. Stellwagen and J. H. Bitter, *Angew. Chemie - Int. Ed.*, 2013, **52**, 5089–5092.
14 M. Lu, F. Lu, J. Zhu, M. Li, J. Zhu and Y. Shan, *React. Kinet. Mech. Catal.*, 2015, **115**, 251–262.
15 J. Han, J. Duan, P. Chen, H. Lou and X. Zheng, *Adv. Synth. Catal.*, 2011, **353**, 2577–2583.
16 S. A. W. Hollak, R. W. Gosselink, D. S. Van Es and J. H. Bitter, *ACS Catal.*, 2013, **3**, 2837–2844.
17 S. K. Kim, D. Yoon, S. C. Lee and J. Kim, *ACS Catal.*, 2015, **5**, 3292–3303.
18 D. R. Stellwagen and J. H. Bitter, *Green Chem.*, 2015, **17**, 582–593.
19 J. Liang, R. Ding, Y. Wu, Y. Chen, K. Wu, Y. Meng, M. Yang and Y. Wang, *J. Mol. Catal. A Chem.*, 2016, **411**, 95–102.
20 Y. Qin, P. Chen, J. Duan, J. Han, H. Lou, X. Zheng and H. Hong, *RSC Adv.*, 2013, **3**, 17485.
21 J. Han, J. Duan, P. Chen, H. Lou, X. Zheng and H. Hong, *ChemSusChem*, 2012, **5**, 727–733.
22 J. Han, J. Duan, P. Chen, H. Lou, X. Zheng and H. Hong, *Green Chem.*, 2011, **13**, 2561.
23 W. S. Lee, Z. Wang, R. J. Wu and A. Bhan, *J. Catal.*, 2014, **319**, 44–53.
24 W. S. Lee, A. Kumar, Z. Wang and A. Bhan, *ACS Catal.*, 2015, **5**, 4104–4114.
25 Q. Lu, C. J. Chen, W. Luc, J. G. Chen, A. Bhan and F. Jiao, *ACS Catal.*, 2016, **6**, 3506–3514.
26 A. A. Smirnov, Z. Geng, S. A. Khromova, S. G. Zavarukhin, O. A. Bulavchenko, A. A. Saraev, V. V. Kaichev, D. Y. Ermakov and V. A. Yakovlev, *J. Catal.*, 2017, **354**, 61–77.
27 T. Iida, M. Shetty, K. Murugappan, Z. Wang, K. Ohara, T. Wakihara and Y. Román-Leshkov, *ACS Catal.*, 2017, **7**, 8147–8151.
28 A. L. Jongerius, R. W. Gosselink, J. Dijkstra, J. H. Bitter, P. C. A. Bruijnincx and B. M.

Weckhuysen, *ChemCatChem*, 2013, **5**, 2964–2972.
29 R. Li, A. Shahbazi, L. Wang, B. Zhang, A. M. Hung and D. C. Dayton, *Appl. Catal. A Gen.*, 2016, **528**, 123–130.
30 E. Santillan-Jimenez, M. Perdu, R. Pace, T. Morgan and M. Crocker, *Catalysts*, 2015, **5**, 424–441.
31 R. Ma, K. Cui, L. Yang, X. Ma and Y. Li, *Chem. Commun.*, 2015, **51**, 10299–10301.
32 J. Chang, T. Danuthai, S. Dewiyanti, C. Wang and A. Borgna, *ChemCatChem*, 2013, **5**, 3041–3049.
33 Z. Cai, F. Wang, X. Zhang, R. Ahishakiye, Y. Xie and Y. Shen, *Mol. Catal.*, 2017, **441**, 28–34.
34 R. Moreira, E. Ochoa, J. Luis Pinilla, A. Portugal and I. Suelves, *Catalysts*, 2018, **8**, 127.
35 K. Xiong, W. S. Lee, A. Bhan and J. G. Chen, *ChemSusChem*, 2014, **7**, 2146–2149.
36 Y. Shi, Y. Yang, Y.-W. Li and H. Jiao, *ACS Catal.*, 2016, **6**, 6790–6803.
37 Z. Jiang, W. Wan, Z. Lin, J. Xie and J. G. Chen, *ACS Catal.*, 2017, **7**, 5758–5765.
38 W. Wan, Z. Jiang and J. G. Chen, *Top. Catal.*, , DOI:10.1007/s11244-018-0901-x.
39 R. B. Levy and M. Boudart, *Science (80-. ).*, 1973, **181**, 547–549.
40 S. T. Oyama, *Catal. Today*, 1992, **15**, 179–200.
41 C. C. Tripathi, M. Kumar and D. Kumar, *Appl. Surf. Sci.*, 2009, **255**, 3518–3522.
42 Z. Lin, W. Wan, S. Yao and J. G. Chen, *Appl. Catal. B Environ.*, 2018, **233**, 160–166.
43 M. M. Sullivan, C.-J. Chen and A. Bhan, *Catal. Sci. Technol.*, 2016, **6**, 602–616.
44 A. M. Robinson, J. E. Hensley and J. Will Medlin, *ACS Catal.*, 2016, **6**, 5026–5043.
45 W. Yu, Z. J. Mellinger, M. A. Barteau and J. G. Chen, *J. Phys. Chem. C*, 2012, **116**, 5720–5729.
46 M. Siaj, C. Reed, S. T. Oyama, S. L. Scott and P. H. McBreen, *J. Am. Chem. Soc.*, 2004, **126**, 9514–9515.
47 H. H. Hwu and J. G. Chen, *J. Phys. Chem. B*, 2003, **107**, 2029–2039.
48 A. P. Farkas and F. Solymosi, *Surf. Sci.*, 2007, **601**, 193–200.
49 T. G. Kelly and J. G. Chen, *Green Chem.*, 2014, **16**, 777–784.
50 Z. Chen, S. S. Perry, A. Savan, P. M. Adams and S. V. Didziulis, *J. Vac. Sci. Technol. A Vacuum, Surfaces, Film.*, 2005, **23**, 234.
51 R. L. Guenard, L. C. Fernández-Torres, B. Il Kim, S. S. Perry, P. Frantz and S. V. Didziulis, *Surf. Sci.*, 2002, **515**, 103–116.
52 A. P. Farkas and F. Solymosi, *Surf. Sci.*, 2008, **602**, 1475–1485.
53 H. Ren, D. A. Hansgen, A. L. Stottlemyer, T. G. Kelly and J. G. Chen, *ACS Catal.*, 2011, **1**, 390–398.
54 J. B. Benziger, E. I. Ko and R. J. Madix, *J. Catal.*, 1980, **64**, 132–142.
55 J. B. Benziger, E. I. Ko and R. J. Madix, *J. Catal.*, 1979, **58**, 149–153.
56 W. Yu, M. A. Barteau and J. G. Chen, *J. Am. Chem. Soc.*, 2011, **133**, 20528–20535.
57 J. R. McManus and J. M. Vohs, *Surf. Sci.*, 2014, **630**, 16–21.
58 H. H. Hwu, J. G. Chen, K. Kourtakis and J. G. Lavin, *J. Phys. Chem. B*, 2001, **105**, 10037–10044.
59 K. Xiong, W. Yu and J. G. Chen, *Appl. Surf. Sci.*, 2014, **323**, 88–95.
60 S. K. Kim, J. Kim and S. C. Lee, *Catal. Commun.*, 2017, **99**, 61–65.
61 A. S. Rocha, L. A. Souza, R. R. Oliveira, A. B. Rocha and V. Teixeira da Silva, *Appl. Catal. A Gen.*, 2017, **531**, 69–78.
62 F. G. Baddour, C. P. Nash, J. A. Schaidle and D. A. Ruddy, *Angew. Chemie - Int. Ed.*,

2016, **55**, 9026–9029.
63 S. K. Bej and L. T. Thompson, *Appl. Catal. A Gen.*, 2004, **264**, 141–150.
64 W. Zhang, Y. Zhang, L. Zhao and W. Wei, *Energy and Fuels*, 2010, **24**, 2052–2059.
65 M. M. Sullivan, J. T. Held and A. Bhan, *J. Catal.*, 2015, **326**, 82–91.
66 S. Phimsen, W. Kiatkittipong, H. Yamada, T. Tagawa, K. Kiatkittipong, N. Laosiripojana and S. Assabumrungrat, *Energy Convers. Manag.*, 2017, **151**, 324–333.
67 Y. Qin, L. He, J. Duan, P. Chen, H. Lou, X. Zheng and H. Hong, *ChemCatChem*, 2014, **6**, 2698–2705.
68 J. C. Serrano-Ruiz and J. A. Dumesic, *Energy Environ. Sci.*, 2011, **4**, 83–99.
69 V. Teixeira da Silva and L. A. Sousa, in *The role of catalysis for the sustainable production of bio-fuels and bio-chemicals*, eds. K. S. Triantafyllidis, A. A. Lappas and M. Stöcker, Elsevier, 1st edn., 2013, pp. 67–92.
70 A. A. Rosatella, S. P. Simeonov, R. F. M. Frade and C. A. M. Afonso, *Green Chem.*, 2011, **13**, 754.
71 M. Siaj, I. Temprano, N. Dubuc and P. H. McBreen, *J. Organomet. Chem.*, 2006, **691**, 5497–5504.
72 N. Dubuc and P. H. McBreen, *Top. Catal.*, 2015, **58**, 232–239.
73 Y. He and S. Laursen, *ACS Catal.*, 2017, **7**, 3169–3180.
74 R. Liu, M. Pang, X. Chen, C. Li, C. Xu and C. Liang, *Catal. Sci. Technol.*, 2017, **7**, 1333–1341.
75 W.-S. Lee, Z. Wang, W. Zheng, D. G. Vlachos and A. Bhan, *Catal. Sci. Technol.*, 2014, **4**, 2340.
76 C. J. Chen and A. Bhan, *ACS Catal.*, 2017, **7**, 1113–1122.
77 C. J. Chen, W. S. Lee and A. Bhan, *Appl. Catal. A Gen.*, 2016, **510**, 42–48.
78 S. Boullosa-Eiras, R. Lødeng, H. Bergem, M. Stöcker, L. Hannevold and E. A. Blekkan, *Catal. Today*, 2014, **223**, 44–53.
79 P. M. Mortensen, H. W. P. De Carvalho, J. D. Grunwaldt, P. A. Jensen and A. D. Jensen, *J. Catal.*, 2015, **328**, 208–215.
80 T. Dai, C. Li, L. Li, Z. K. Zhao, B. Zhang, Y. Cong and A. Wang, *Angew. Chemie - Int. Ed.*, 2018, **57**, 1808–1812.
81 H. Guo, B. Zhang, Z. Qi, C. Li, J. Ji, T. Dai, A. Wang and T. Zhang, *ChemSusChem*, 2017, **10**, 523–532.
82 H. Guo, B. Zhang, C. Li, C. Peng, T. Dai, H. Xie, A. Wang and T. Zhang, *ChemSusChem*, 2016, **9**, 3220–3229.
83 M. Grilc, G. Veryasov, B. Likozar, A. Jesih and J. Levec, *Appl. Catal. B Environ.*, 2015, **163**, 467–477.
84 J. Engelhardt, P. Lyu, P. Nachtigall, F. Schüth and Á. M. García, *ChemCatChem*, 2017, **9**, 1985–1991.
85 L. He, Y. Qin, H. Lou and P. Chen, *RSC Adv.*, 2015, **5**, 43141–43147.
86 H. Wang, S. Liu and K. J. Smith, *Energy and Fuels*, 2016, **30**, 6039–6049.
87 H. Wang, S. Liu, B. Liu, V. Montes, J. M. Hill and K. J. Smith, *J. Solid State Chem.*, 2018, **258**, 818–824.
88 E. I. Ko and R. J. Madix, *Surf. Sci.*, 1980, **100**, L449–L453.
89 E. I. Ko and R. J. Madix, *Surf. Sci.*, 1981, **109**, 221–238.
90 T. Prasomsri, M. Shetty, K. Murugappan and Y. Román-Leshkov, *Energy Environ. Sci.*, 2014, **7**, 2660–2669.

91 K. Li, R. Wang and J. Chen, *Energy and Fuels*, 2011, **25**, 854–863.
92 M. Á. González-Borja and D. E. Resasco, *Energy & Fuels*, 2011, **25**, 4155–4162.
93 L. Souza Macedo, D. R. Stellwagen, V. Teixeira Da Silva and J. H. Bitter, *ChemCatChem*, 2015, **7**, 2816–2823.
94 M. D. Porosoff, X. Yang, J. A. Boscoboinik and J. G. Chen, *Angew. Chemie - Int. Ed.*, 2014, **53**, 6705–6709.
95 Y. Kwon, K. J. P. Schouten, J. C. Van Der Waal, E. De Jong and M. T. M. Koper, *ACS Catal.*, 2016, **6**, 6704–6717.
96 W. Wan, B. M. Tackett and J. G. Chen, *Chem. Soc. Rev.*, 2017, **46**, 1807–1823.
97 B. M. Tackett, W. Sheng and J. G. Chen, *Joule*, 2017, **1**, 253–263.
98 M. Grilc, B. Likozar and J. Levec, *ChemCatChem*, 2016, **8**, 180–191.
99 B. Hočevar, M. Grilc, M. Huš and B. Likozar, *Appl. Catal. B Environ.*, 2017, **218**, 147–162.
100 M. Grilc and B. Likozar, *Chem. Eng. J.*, 2017, **330**, 383–397.
101 K. Momma and F. Izumi, *J. Appl. Crystallogr.*, 2011, **44**, 1272–1276.

**Table 1.** HDO of linear chain oxygenates over TMC surfaces

| **Reactant** | **Catalyst** | **Technique** | **Ref.** |
|---|---|---|---|
| acetaldehyde | Ni/WC | DFT, TPD, HREELS | 45 |
| acetaldehyde | β-$Mo_2C$ | RAIS | 46 |
| acetaldehyde | WC | DFT, TPD, HREELS | 45 |
| acetic acid | Ni/WC | DFT, TPD, HREELS | 45 |
| acetic acid | WC | DFT, TPD, HREELS | 45 |
| acetone | $Mo_2C$ | DFT, TPD | 10 |
| CO | C/W(110) | AES, TPD, HREELS | 47 |
| ethanol | $Mo_2C$/Mo(100) | Work function, TPD, HREELS | 48 |
| ethanol | $Mo_2C$ | DFT, TPD, HREELS | 49 |
| ethanol | TiC | TPD | 50 |
| ethanol | TiC(100) | TPD | 50 |
| ethanol | TiC(100) | TPD, HREELS | 51 |
| ethanol | VC(100) | TPD, HREELS | 51 |
| ethanol | K/$Mo_2C$/Mo(100) | Work function, TPD, HREELS | 52 |
| ethanol | Ni/WC | DFT, TPD, HREELS | 53 |
| ethanol | Ni/$Mo_2C$ | DFT, TPD, HREELS | 49 |
| ethylene glycol | WC | TPD, HREELS | 45 |
| ethylene glycol | Ni/WC | DFT, TPD, HREELS | 45 |
| formaldehyde | C/W(100) | TPRS | 54 |
| formic acid | C/W(100) | TPRS | 55 |
| glycoaldehyde | Ni/WC | DFT, TPD, HREELS | 56 |
| glycoaldehyde | $Mo_2C$/Mo(100) | TPD, HREELS | 57 |
| methanol | C/W(111) | TPD, HREELS | 58 |
| propanal | $Mo_2C$/Mo(1 1 0) | TPD, HREELS | 59 |
| propanal | WC | DFT, TPD, HREELS | 9 |
| propanol | WC | DFT, TPD, HREELS | 9 |
| Propanoic acid | $Mo_2C$ | DFT | 60 |
| 1-propanol | $Mo_2C$/Mo(1 1 0) | TPD, HREELS | 59 |

**Table 2**. Vapor-phase HDO of linear chain oxygenates over powder TMC catalysts

| **Reactant** | **Catalyst** | **T(K)** | **P(MPa)** | **$H_2$/oxygenate ratio** | **Characterization Techniques** | **Ref.** |
|---|---|---|---|---|---|---|
| acrylic acid | $Mo_2C/Al_2O_3$ | 298-673 | 0.10 | -- | DRIFTS, TPSR | 61 |
| acetic acid | α-$MoC_{1-x}$ in SBA-15 silica | 298-873 | 0.13-0.15 | 6 | XRD, TEM, TPD | 62 |
| acetic acid | $Mo_2C$ | 298-873 | 0.10 | 3.9 | XRD, $N_2$ adsorption, $H_2$ Chemisorption, TPD, XPS, DRIFTS | 11 |
| acetone | $Mo_2C$ | 573 | 0.1 | 10 | XRD, SEM, TEM | 10 |
| acetone | $Mo_2C$ | 369 | 0.01-0.082 | 324 | XRD, CO chemisorption, $N_2$ adsorption, XPS, TEM | 12 |
| acetone | $Mo_2C$ | 483 | 0.1 | 9.75 | $N_2$ adsorption, TPD, TGA | 63 |
| acetone | NiMo carbide | 493-573 | 0.1-5 | -- | XRD, TPR, TPO, TPD | 64 |
| acetaldehyde | NiMo carbide | 493-573 | 0.1-5 | -- | XRD, TPR, TPO, TPD | 64 |
| isopropanol | $Mo_2C$ | 403-438 | 0.10-0.13 | -- | $N_2$ adsorption, CO chemisorption, XRD, XPS, TEM, HAADF-STEM, | 65 |
| oleic acid | $Mo_2C$/RGO | 623 | 5 | 4.5 | ICP-AES, XPS, XRD, FE-SEM, HR-TEM, $N_2$ adsorption, CO chemisorption | 17 |
| propanal | $Mo_2C$ | 573 | 0.1 | 10 | XRD, SEM, TEM | 10 |
| propanol | $Mo_2C$ | 573 | 0.1 | 10 | XRD, SEM, TEM | 10 |
| propanal | WC | 653 | 0.1 | 10 | XRD, TEM | 9 |
| propanol | WC | 653 | 0.1 | 10 | XRD, TEM | 9 |
| soybean oil | $Mo_2C$/RGO | 623 | 5 | 30 | ICP-AES, XPS, XRD, FE-SEM, HR-TEM, $N_2$ adsorption, CO chemisorption | 17 |
| 2-propanol | $Mo_2C$ | 573 | 0.1 | 10 | XRD, SEM, TEM | 10 |

CNT: carbon nanotube; CNF: carbon nanofiber; AC: activated carbon; MC: mesoporous carbon; OMC: ordered mesoporous carbon; RGO: reduced graphene oxide

**Table 3**. Liquid-phase HDO of linear chain oxygenates over powder TMC catalysts

| **Reactant** | **Catalyst** | **T(K)** | **P(MPa)** | **Solvent** | **Characterization Techniques** | **Ref.** |
|---|---|---|---|---|---|---|
| Coffee oil | NiC | 648-698 | 2-4 | -- | ICP, elemental analysis, FTIR, NMR, XRD, TGA | 66 |
| ethyl caprate | $NiMoC/SiO_2$ | 553-593 | 6 | hexadecane | TPR, $N_2$ adsorption, XRD, XPS, CO chemisorption, elemental analysis | 26 |
| hexadecanamide | β-$Mo_2C$/CNTs | 453 | 4 | decane | XRD, $N_2$ adsorption, XPS, TEM | 19 |
| maize oil | Mo/RGO | 533 | 2 | hexane | $N_2$ adsorption, Raman, SEM, XRD, TEM, EDX, TPD, XPS | 67 |
| maize oil | Mo/AC | 533 | 2 | hexane | $N_2$ adsorption, Raman, SEM, XRD, TEM, EDX, TPD, XPS | 67 |
| maize oil | Mo/G | 533 | 2 | hexane | $N_2$ adsorption, Raman, SEM, XRD, TEM, EDX, TPD, XPS | 67 |
| maize oil | $Mo/C_{60}$ | 533 | 2 | hexane | $N_2$ adsorption, Raman, SEM, XRD, TEM, EDX, TPD, XPS | 67 |
| methyl stearate | $Mo_2C$/MC | 543 | 6 | -- | XRD, $N_2$ adsorption, TEM, TPR, XPS | 14 |
| methyl stearate | $W_2C$/CNF | 623 | 5 | dodecane | $N_2$ adsorption, XRD, Raman, TEM | 13 |
| methyl stearate | $Mo_2C$/AC | 553-573 | 1-2 | hexane | XRD, FE-SEM, Raman, HR-TEM, $N_2$ adsorption, TPD, ICP-AAS | 15 |
| oleic acid | $Mo_2C$/CNF | 623 | 5 | dodecane | $N_2$ adsorption, XRD, TEM, XPS | 16 |
| oleic acid | $W_2C$/CNF | 623 | 5 | dodecane | $N_2$ adsorption, XRD, TEM, XPS | 16 |
| stearic acid | $W_2C$/CNF | 623 | 5 | dodecane | $N_2$ adsorption, XRD, Raman, TEM | 13 |
| stearic acid | $Mo_2C$/CNF | 573-623 | 3-5 | dodecane | XRD, $N_2$ adsorption, | 18 |

| | | | | | | |
|---|---|---|---|---|---|---|
| | | | | | TGA, TEM, XPS | |
| stearic acid | $W_2C$/CNF | 573-623 | 3-5 | dodecane | XRD, $N_2$ adsorption, TGA, TEM, XPS | 18 |
| stearic acid | β-$Mo_2C$/CNTs | 453 | 4 | decane | XRD, $N_2$ adsorption, XPS, TEM | 19 |
| tristearin | $W_2C$/CNF | 623 | 5 | dodecane | $N_2$ adsorption, XRD, Raman, TEM | 13 |
| vegetable oils | $Mo_2C$/CNF | 513-533 | 1-2.5 | hexane | XRD, TEM, TGA, SEM, Raman | 20 |
| vegetable oils | $Mo_2C$/OMC | 533 | 2 | hexane | XRD, TEM, STEM, $N_2$ adsorption, XPS, FE-SEM, Raman, ICP-MS | 21 |
| vegetable oils | $Mo_2C$/CNTs | 493-533 | 0.5-2.5 | hexane | XRD, HAADF-STEM, TEM, EDX, Raman, ICP-AAS, FE-SEM | 22 |
| vegetable oils | $Mo_2C$/AC | 533-573 | 1-2 | hexane | XRD, FE-SEM, Raman, HR-TEM, $N_2$ adsorption, TPD, ICP-AAS | 15 |

**Table 4** HDO of furan and benzene-ring containing oxygenates over TMC surfaces

| **Reactant** | **Catalyst** | **Technique** | **Ref.** |
|---|---|---|---|
| cyclopentanone | β-$Mo_2C$ | RAIS | 71 |
| cyclobutanone | β-$Mo_2C$ | RAIS, TPD, XPS | 72 |
| cyclopentanone | β-$Mo_2C$ | RAIS, TPD, XPS | 72 |
| cyclohexanone | β-$Mo_2C$ | RAIS, TPD, XPS | 72 |
| furfural | $Mo_2C$ | DFT, TPD, HREELS | 35 |
| furfural | $Mo_2C$/Mo(100) | TPD, HREELS | 57 |
| furfural | $Mo_2C$(101) | DFT | 36 |
| furfural | $Mo_2C$/Mo(110) | TPD, HREELS | 59 |
| furfuryl alcohol | $Mo_2C$ | DFT, TPD, HREELS | 35 |
| furfuryl alcohol | $Mo_2C$/Mo(110) | TPD, HREELS | 59 |
| guaiacol | TiC | DFT | 73 |
| guaiacol | $Ni_3C$ | DFT | 73 |

**Table 5** Adsorption Energies $E_{ads}$ (eV) of Surface Intermediates on the Clean $Mo_2C(101)$ Surface (PBE values are listed in parentheses) . Adapted from Shi *et al.* [36] with permission. Copyright 2016 American Chemical Society.

| Config. | $E_{ads}$ |
|---|---|
| cis-F-CHO | -2.68 (-1.78) |
| trans-F-CHO | -2.50 (-1.57) |
| F-$CH_2OH$ | -2.23 (-1.27) |
| F-$CH_3$ | -1.82 (-0.97) |
| F-H | -1.58 (0.88) |

**Table 6** – Energy Barrier $E_a$ (eV), Reaction Energy $E_r$ (eV), and Rate Constant k (423 K) of Furfural HDO on the Clean and 4H Pre-covered $Mo_2C(101)$ Surfaces from Microkinetic Modeling. Adapted from Shi *et al.* [36] with permission. Copyright 2016 American Chemical Society.

| | Clean $Mo_2C(101)$ surface | | | 4H precovered $Mo_2C(101)$ | | |
|---|---|---|---|---|---|---|
| Reaction | $E_a$ | $E_r$ | k | $E_a$ | $E_r$ | k |
| F-CHO + H = $FCH_2O$ | 1.11 | 0.12 | $3.95*10^{-1}$ | 1.21 | -0.07 | $2.39*10^{-2}$ |
| F-CHO + H = F-CO + 2H | 0.97 | 0.07 | $2.14*10^{1}$ | 1.52 | 1.05 | $7.09*10^{-6}$ |

**Table 7** Vapor-phase HDO of furan and benzene-ring containing oxygenates over TMC powder catalysts

| **Reactant** | **Catalyst** | **T(K)** | **P(MPa)** | **$H_2$/oxygenate ratio** | **Characterization Techniques** | **Ref.** |
|---|---|---|---|---|---|---|
| anisole | $Mo_2C$ | 420-520 | 0.1 | 713 | XRD, TEM, $N_2$ adsorption, CO chemisorption, $H_2$ chemisorption | 23 |
| anisole | $Mo_2C$ | 408-438 | 0.1 | 110 | XRD, CO chemisorption, $N_2$ adsorption, CO titration, TPSR | 24 |
| anisole | mesporous $Mo_2C$ | 423-444 | 0.11-0.13 | 666-1666 | XPS, TEM, XAS, CO titration | 25 |
| anisole | mesporous $W_2C$ | 423-444 | 0.11-0.13 | 666-1666 | SEM, TEM, XRD, XPS, $N_2$ adsorption, XAS, CO titration | 25 |
| anisole | $MoC_x$/FAU | 523 | 0.1 | 127 | XRD, $N_2$ adsorption, CO chemisorption, $NH_3$-TPD, TEM, XPS, TGA, HEXTS | 27 |
| benzofuran | $W_2C$ nanorods | 613 | 4 | 1000 | XRD, SEM, TEM, EDX, Raman, $N_2$ adsorption, XPS, TG | 74 |
| ethyl benzoate | NiMo carbide | 493-573 | 0.1-5 | -- | XRD, TPR, TPO, TPD | 64 |
| furfural | $Mo_2C$ | 423 | 0.1 | 405 | XRD, TEM, $N_2$ adsorption, CO chemisorption | 75 |
| guaiacol | Mo/AC | 623-673 | 4 | 20 | TPR, XPS, XRD, FTIR | 32 |
| *m*-cresol | $Mo_2C$ | 423 | 0.1 | 2800 | $N_2$ adsorption, XRD, CO chemisorption, XPS, TPSR, CO titration | 76 |
| phenolic compound mixtures | $Mo_2C$ | 553 | 0.11 | 3300 | XRD, CO chemisorption, $N_2$ adsorption | 77 |
| phenol | $Mo_2C/TiO_2$ | 623-723 | 2.5 | -- | XRD, $N_2$ adsorption, TPR, TGA-MS, CO chemisorption | 78 |
| phenol/octanol mixture | $Mo_2C/ZrO_2$ | 553-653 | 10 | -- | In situ XRD, in situ XAS | 79 |
| 4-methyl-3-cyclohexene-1-carbonylaldehyde | $W_2C$/AC | 573-648 | 0.1 | -- | XRD, XPS, STEM, Microcalorimetry, Raman, $H_2$-TPR-MS, ATR-IR | 80 |

HCS: hollow carbon spheres, FAU: faujasite, HEXTS : high-energy X-ray total scattering

**Table 8** Liquid-phase HDO of furan and benzene-ring containing oxygenates over TMC powder catalysts

| Reactant | Catalyst | T(K) | P(MPa) | Solvent | Characterization Techniques | Ref. |
|---|---|---|---|---|---|---|
| anisole | $NiMoC/SiO_2$ | 553-593 | 6 | hexadecane | TPR, $N_2$ adsorption, XRD, XPS, CO chemisorption, elemental analysis | 26 |
| guaiacol | $Mo_2C$@C Graphite encapsulated $Mo_2C$ core/shell | 573-613 | 0.1-2.8 | methanol | XRD, SEM, EDX, HR-TEM, FTIR, ICP-OES, elemental analysis, TGA, $N_2$ adsorption | 29 |
| guaiacol | $MoC_{1-x}$/AC | 573-623 | 4.0-13.8 | water, dodecane | XRD, $N_2$ adsorption, ICP-OES, CO chemisorption, SEM, EDX | 30 |
| guaiacol | $MoC_{1-x}$/CNT, | 573-623 | 4.0-13.8 | water, dodecane | XRD, $N_2$ adsorption, ICP-OES, CO chemisorption, SEM, EDX | 30 |
| guaiacol | $MoC_{1-x}$/CNF | 573-623 | 4.0-13.8 | water, dodecane | XRD, $N_2$ adsorption, ICP-OES, CO chemisorption, SEM, EDX | 30 |
| guaiacol | a-$MoC_{1-x}$/AC | 553-613 | 0.1 | ethanol | $N_2$ adsorption, XRD, laser light scattering, TGA, Raman | 31 |
| guaiacol | $W_2C$/CNF | 573-648 | 5-6 | dodecane | $N_2$ adsorption, XRD, TEM | 28 |
| guaiacol | $Mo_2C$/CNF | 573-648 | 5-6 | dodecane | $N_2$ adsorption, XRD, TEM | 28 |
| guaiacol | $Mo_2C$/AC | 553-613 | 3 | Tetradecane, Dodecane, Decalin, Tetralin and Ethanol | $H_2$-TPR, XRD, XPS, TEM, $N_2$ adsorption | 33 |
| guaiacol | $Mo_2C$/CNF | 573-623 | 2-3 | decane | XRD, TEM, EDX, $N_2$ adsorption, TPD | 34 |
| lignin | $W_2C$/AC | 523 | 0.69 | methanol | Elemental analysis, GPC, FTIR, $N_2$ adsorption, NMR | 81 |
| lignin | $W_2C$/AC | 473-553 | 0.69 | methanol | ICP-AES, XRD, Raman, GPC, NMR | 82 |
| lignocellulosic | $Mo_2C$ | 573 | 8 | tetralin | Raman, FE-SEM, HR-TEM, EDX, elemental analysis, $N_2$ adsorption, XRD | 83 |
| phenol | MoCx/HCS | 623 | 8 | n-octane | TEM, XRD, $N_2$ adsorption, EDX | 84 |
| Vanillin | $Mo_2C$/AC | 353-453 | 0.6-2 | water | XRD, TEM, TPD | 85 |
| 4-methyl phenol (4-MP) | $Mo_2C/MoO_xC_y$ | 598-648 | 4.3 | decalin | CO uptake, TEM, XRD, XPS | 86 |
| 4-methyl phenol (4-MP) | $Mo_2C$/AC | 623 | 4.3 | decalin | $N_2$ adsorption, XPS, TEM | 87 |

# Schemes

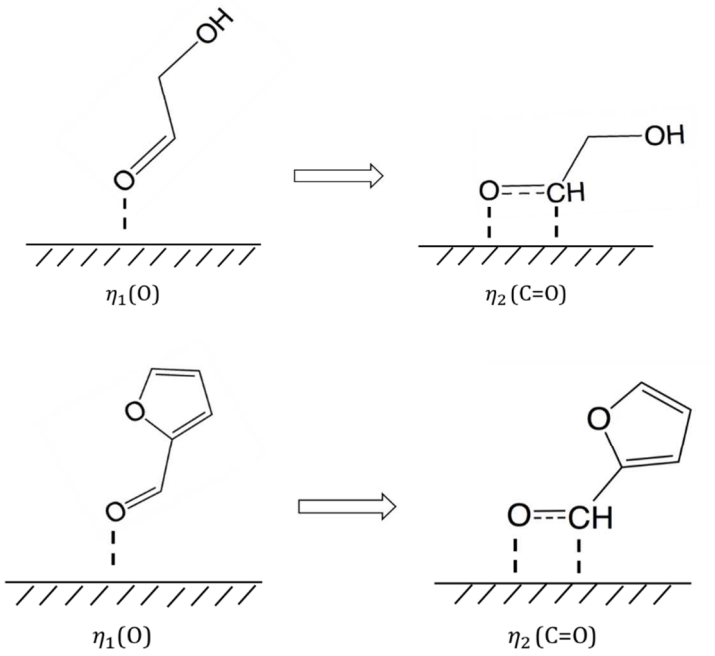


**Scheme 1** Transition of the glycolaldehyde and furfural binding configurations on $Mo_2C$/Mo(110) from $\eta_1(O)$ to di-σ $\eta_2$ (C=O).

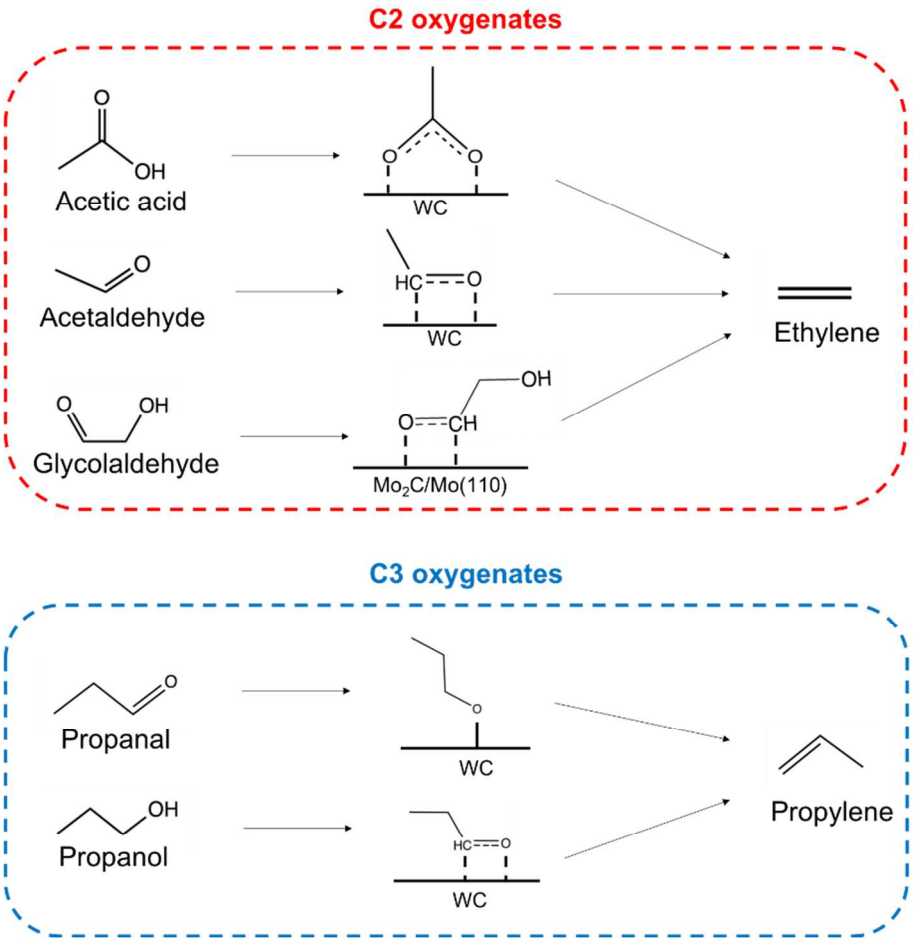


**Scheme 2** Summary of the reaction pathways and proposed intermediates of C2 and C3 oxygenates over WC and $Mo_2C$ surfaces based on Yu *et al.*,[45] McManus *et al.*,[57] and Ren *et al.*.[9]

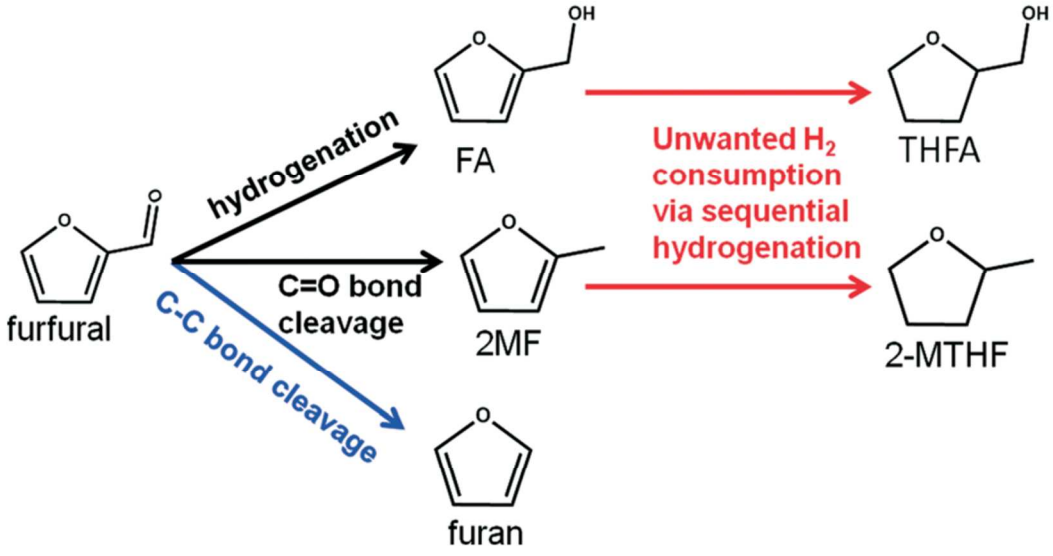


**Scheme 3** Possible reaction pathways for furfural conversion in the presence of $H_2$. FA: furfuryl alcohol, 2MF: 2-methylfuran, THFA: tetrahydrofuran, 2-MTHF: 2-methyltetrahydrofuran. Reprinted from Lee *et al.*[75] with permission from the Royal Society of Chemistry.

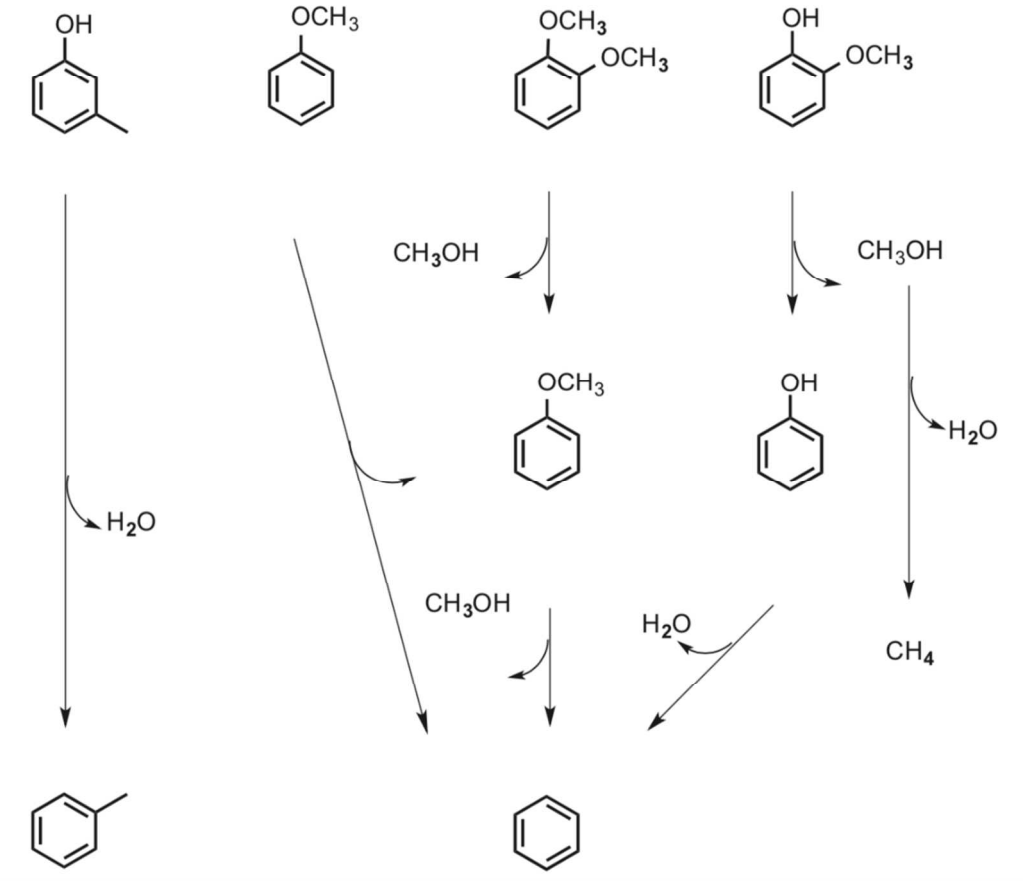


**Scheme 4** Reaction pathways for HDO of lignin-derived phenolic compound mixtures comprising m-cresol, anisole, 1,2-dimethoxybenzene, and guaiacol on $Mo_2C$ catalysts. Reprinted from Bhan *et al.*[77] with permission from Elsevier.

# Figures

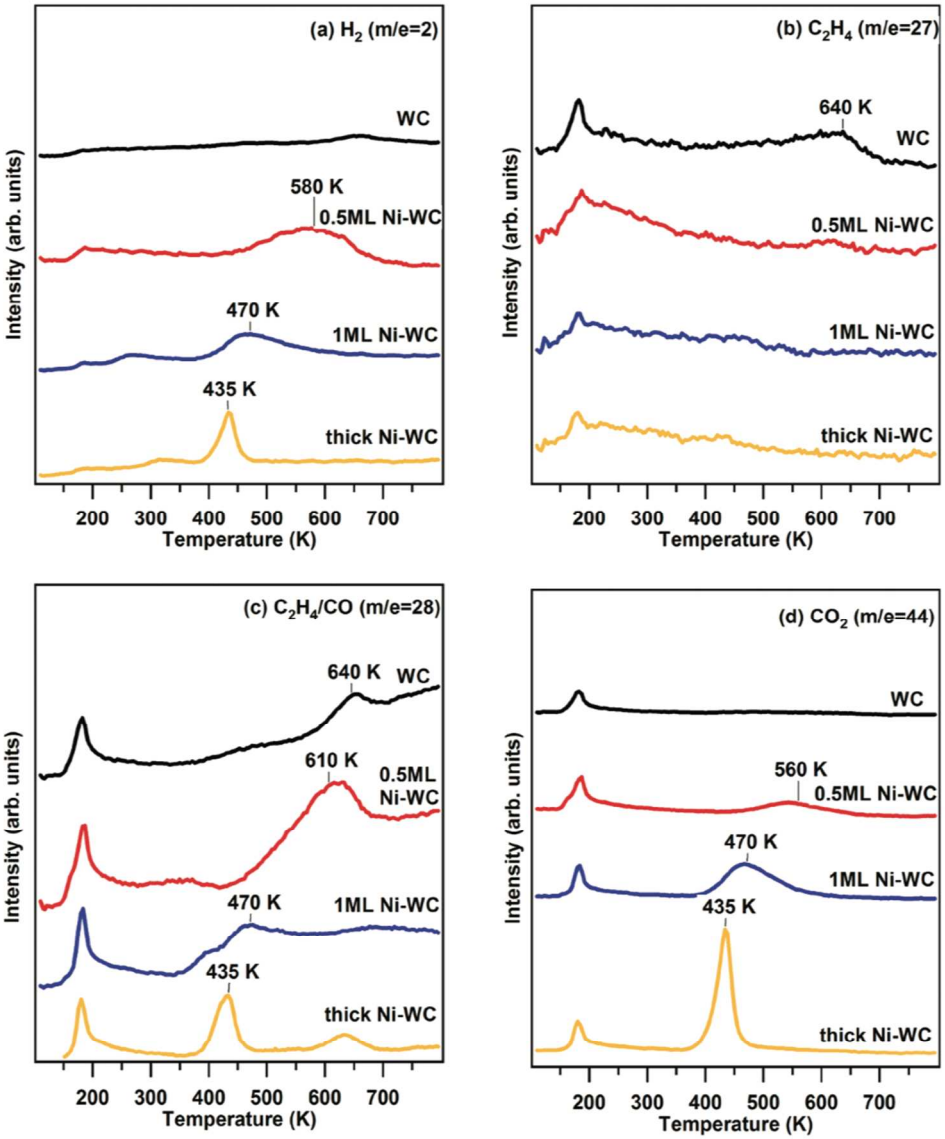


**Fig. 1** TPD spectra of (a) $H_2$, (b) $C_2H_4$ (m/e = 27), (c) $C_2H_4$/CO (m/e = 28), and (d) $CO_2$ with 6 L acetic acid exposure on WC and Ni–WC surfaces. Reprinted from Yu *et al.*[45] with permission. Copyright 2012 American Chemical Society.

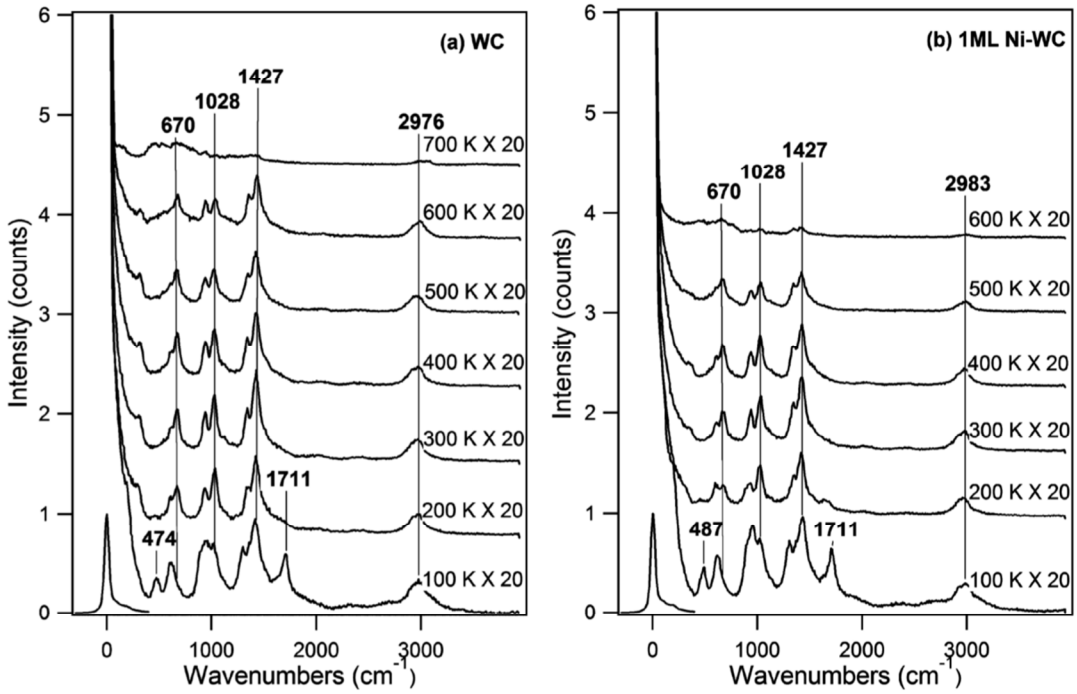


**Fig. 2** HREEL spectra of 8 L acetic acid exposed on (a) WC and (b) 1 ML Ni–WC. Reprinted from Yu *et al.*[45] with permission. Copyright 2012 American Chemical Society.

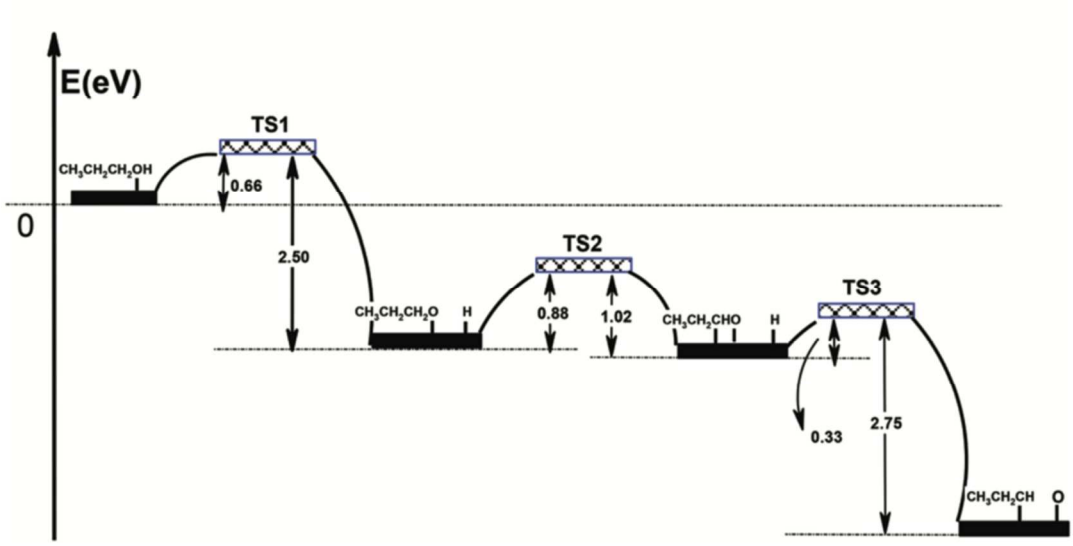


**Fig. 3** Energy profile of the most favorable reaction pathway for propanol decomposition on the WC(0001) surface. Reprinted from Ren *et al.*[9] with permission from the Royal Society of Chemistry.

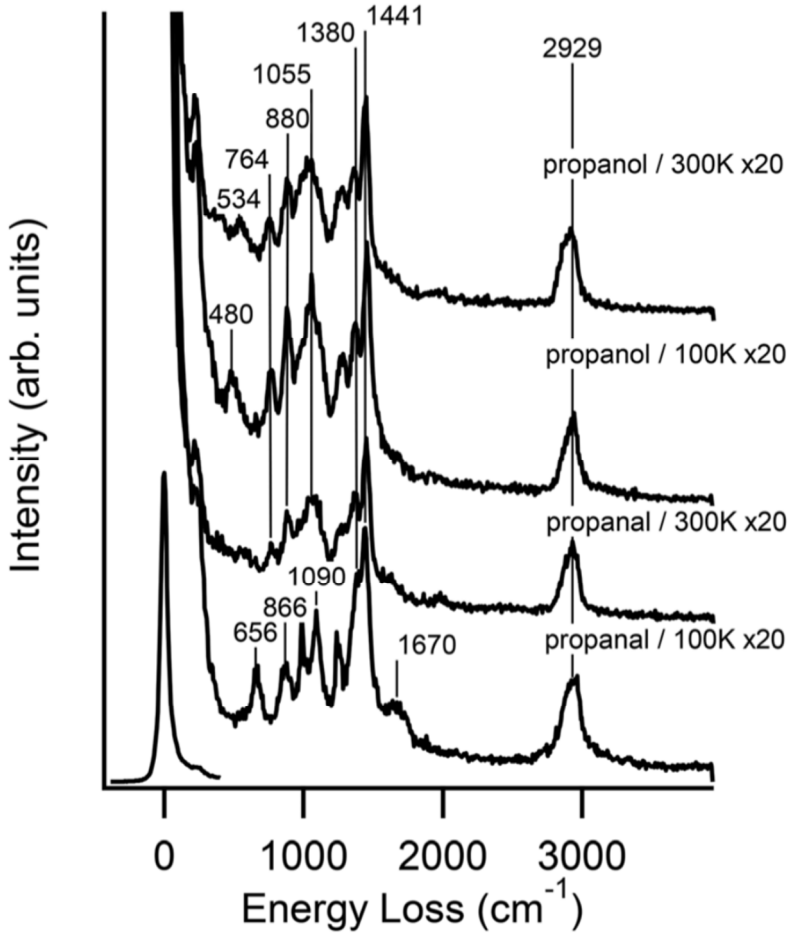


**Fig. 4** HREELS spectra from exposure of the WC surface to propanol or propanal. Reprinted from Ren *et al.*[9] with permission from the Royal Society of Chemistry.

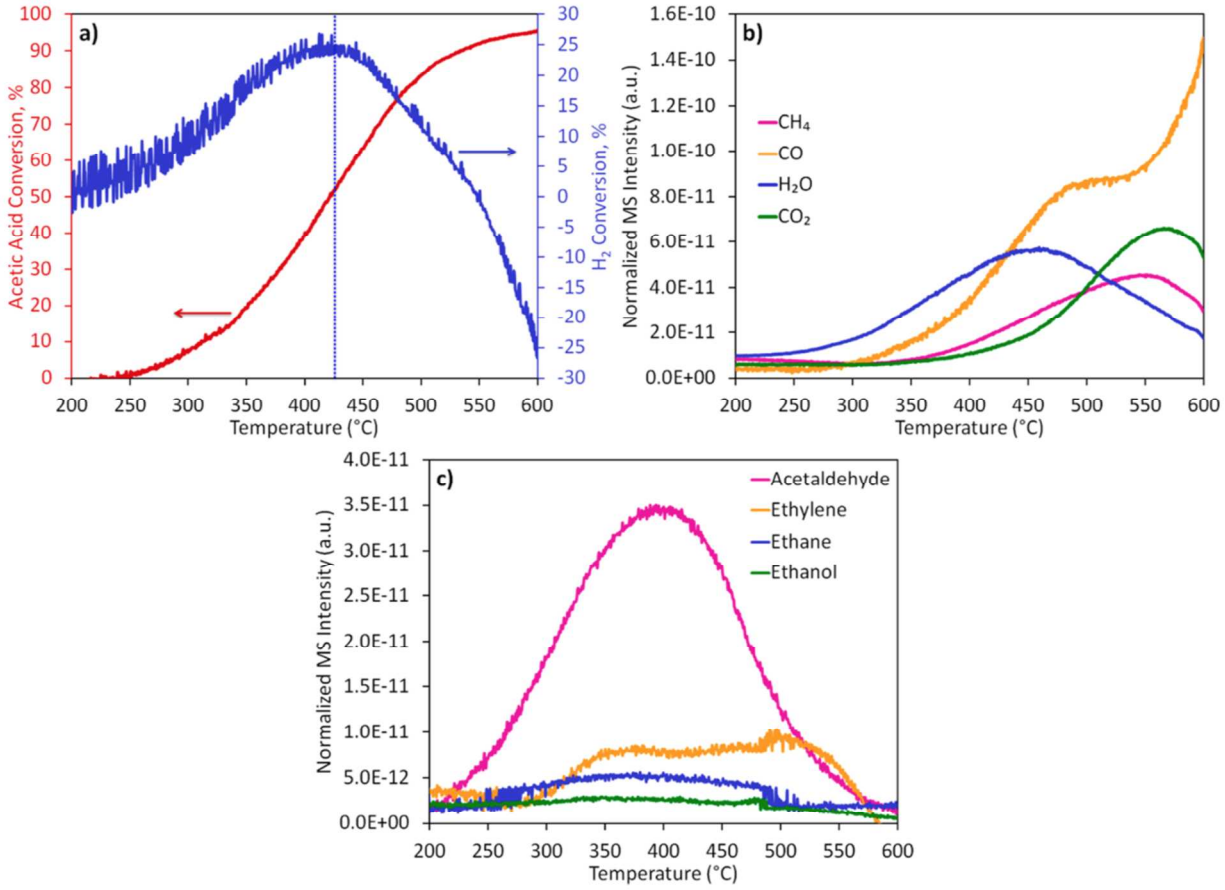


**Fig. 5** Conversion of (a) acetic acid and hydrogen and production of (b) $CH_4$, CO, $H_2O$, and $CO_2$ and (c)HDO products (acetaldehyde, ethanol, ethylene, and ethane) over $Mo_2C$ during acetic acid TPRxn experiments. Positive values of $H_2$ conversion correspond to $H_2$ consumption while negative values correspond to $H_2$ evolution. Reprinted from Schaidle *et al.*[11] with permission. Copyright 2016 American Chemical Society.

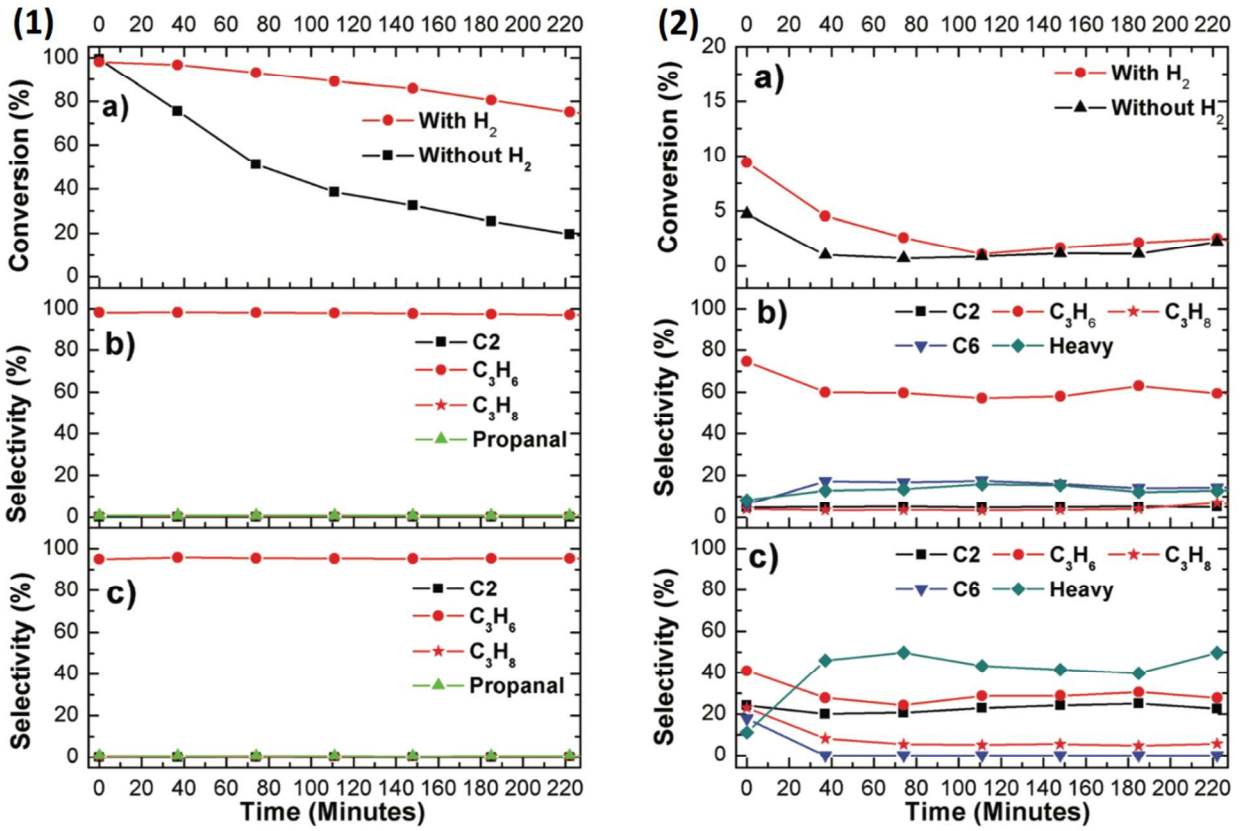


**Fig. 6** Flow reactor results of (1) propanol and (2) propanal deoxygenation reactions at 653 K over WC (reaction conditions: $H_2$–propanol/propanal = 10 : 1, catalyst 43.5 mg): (a) conversion; (b) selectivity with co-feed $H_2$; and (c) selectivity without co-feed $H_2$. Reprinted from Ren *et al.*[9] with permission from the Royal Society of Chemistry.

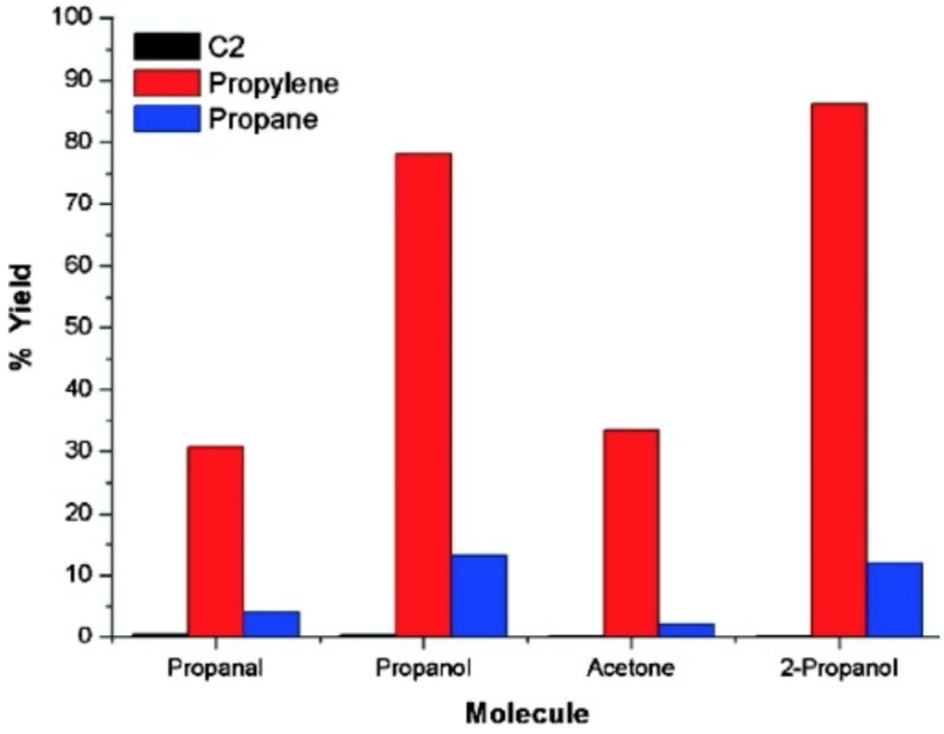


**Fig. 7** Comparison of C2 and C3 yields from different C3 oxygenates with co-feed $H_2$ at 573 K over $Mo_2C$. Reprinted from Ren *et al.*[10] with permission from Wiley.

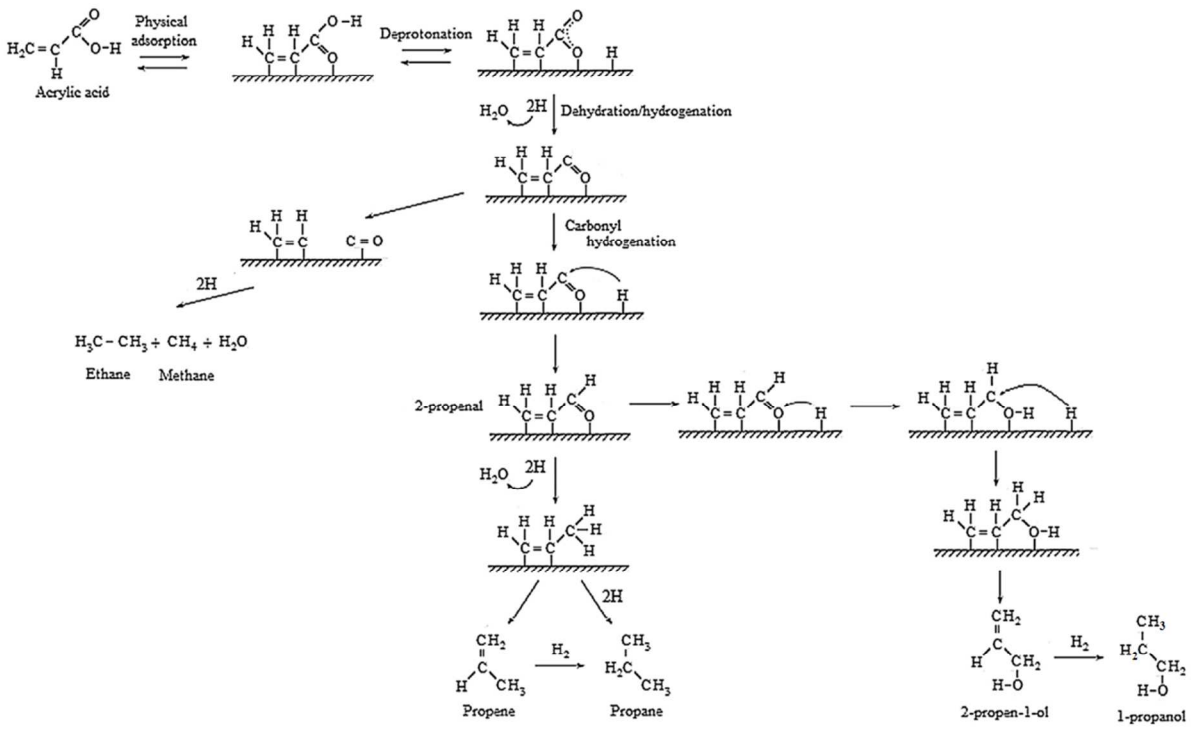


**Fig. 8** Proposed reaction network for acrylic acid HDO on β-$Mo_2C/Al_2O_3$. Reprinted from Rocha *et al.*[61] with permission from Elsevier.

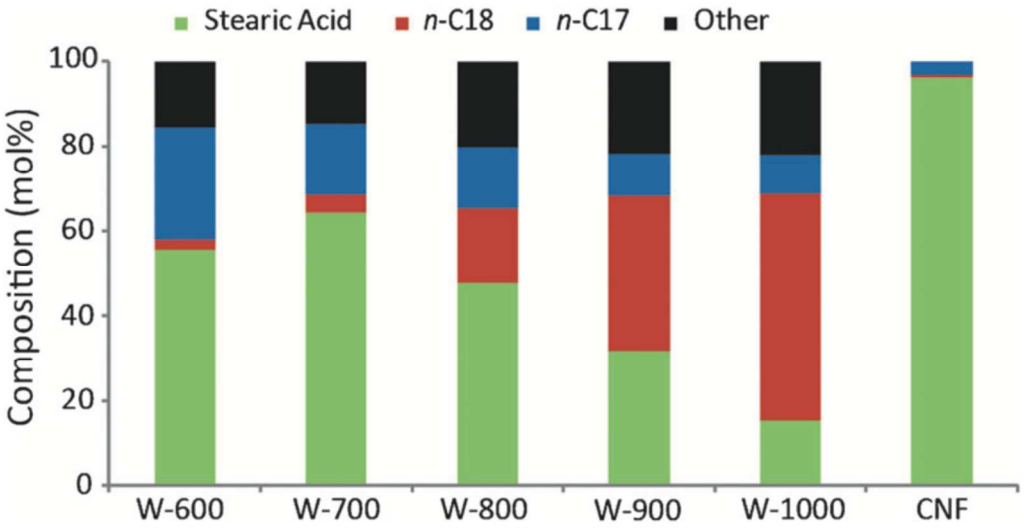


**Fig. 9** Composition of the reaction mixture after the deoxygenation of stearic acid by various tungsten-based catalysts. Bare CNFs are included as a reference. Reaction conditions: T = 623 K, P = 5 MPa $H_2$, t = 5h, $m_{stearic\ acid}$ = 2g, $m_{cat}$ = 0.25 g, $m_{dodecane}$ = 36 g. Reprinted from Bitter *et al.*[13] with permission from Wiley.

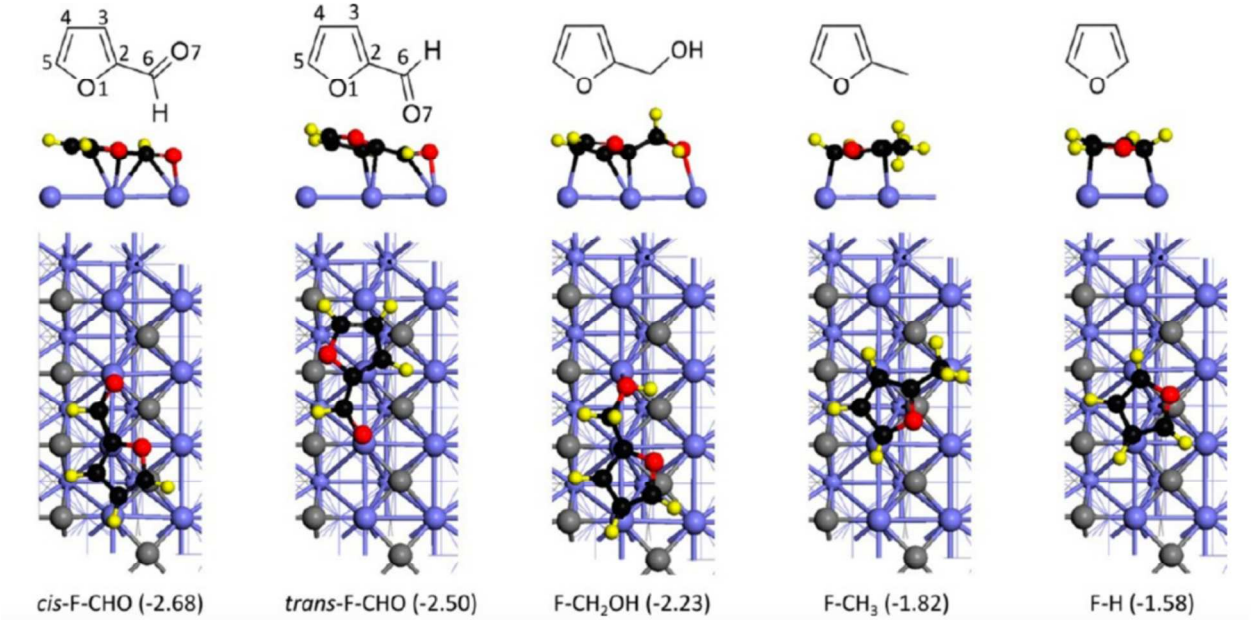


**Fig. 10** Top and side views of the adsorption configurations of surface intermediates as well as the adsorption energy (eV) on the clean $Mo_2C(101)$ surface (Mo, blue; bulk C, gray; adsorbed C, black; H, yellow; O, red; F = 2-furanyl). Reprinted from Shi *et al.*[36] with permission. Copyright 2016 American Chemical Society.

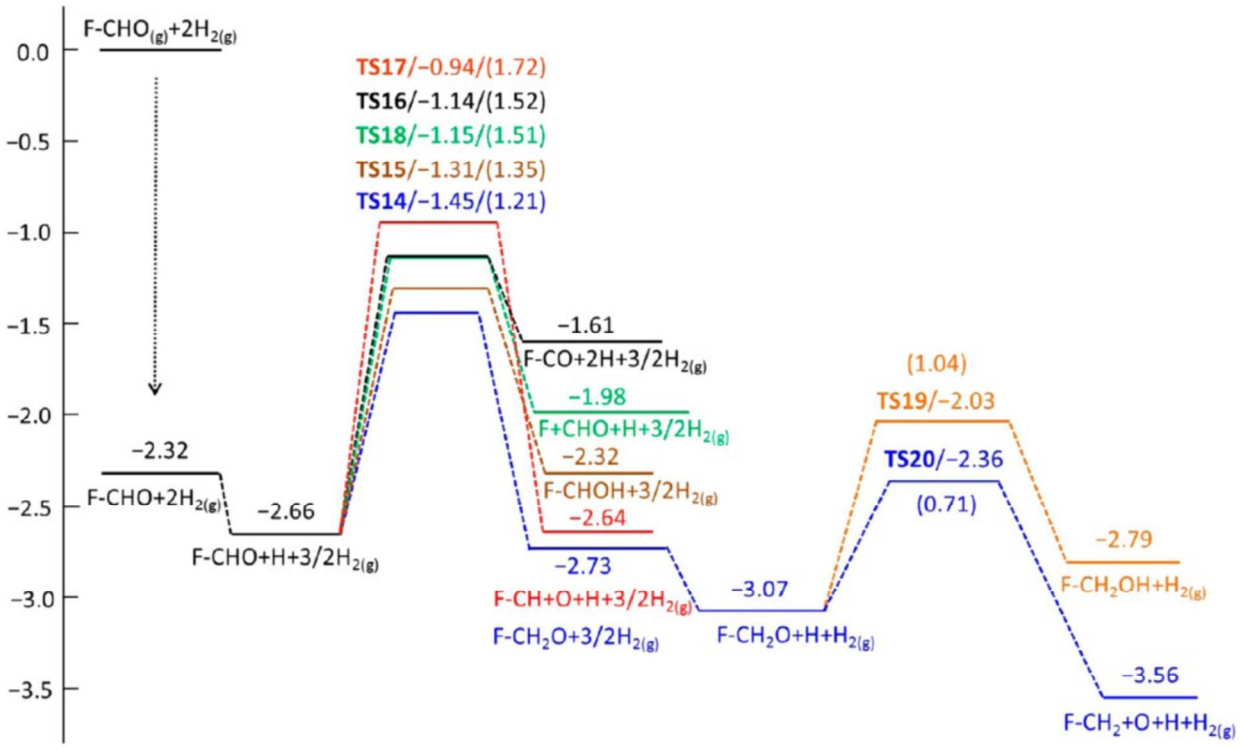


**Fig. 11** Potential energy surfaces (in eV) for the reaction routes on the 4H precovered $Mo_2C$(101) surface (F = 2-furanyl). Reprinted from Shi *et al.*[36] with permission. Copyright 2016 American Chemical Society.

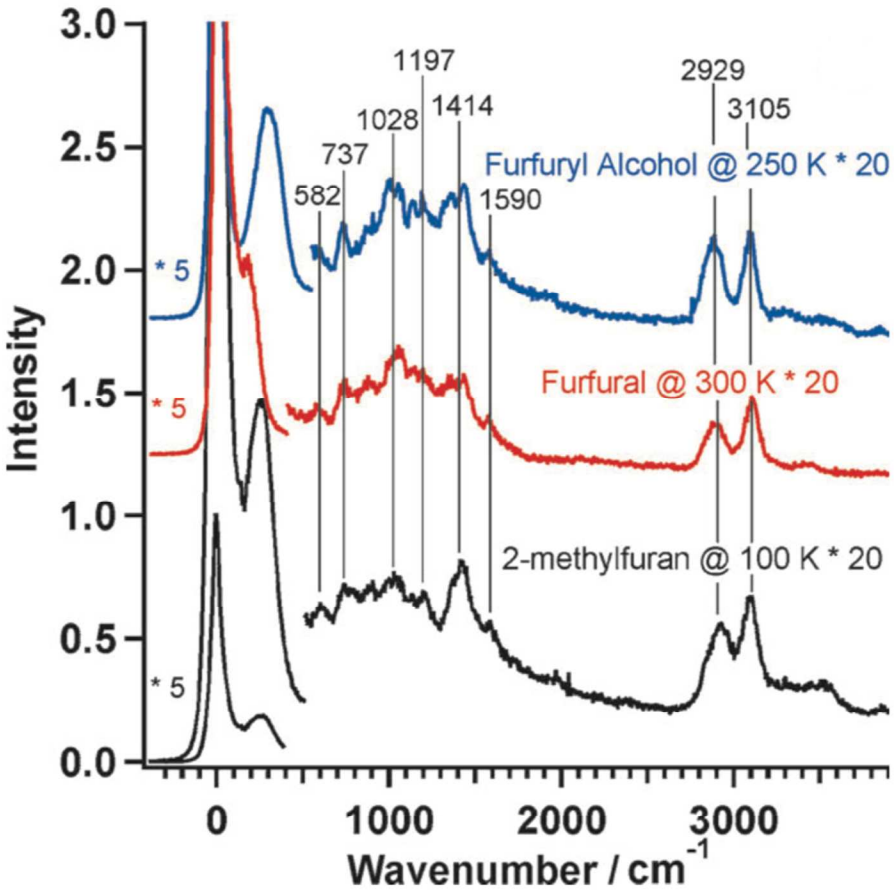


**Fig. 12** HREELS of furfural (red), 2-methylfuran (black) and furfuryl alcohol (blue) adsorbed onto $Mo_2C$ after annealing the surface to various temperatures. Reprinted from Xiong *et al.*[35] with permission from Wiley.

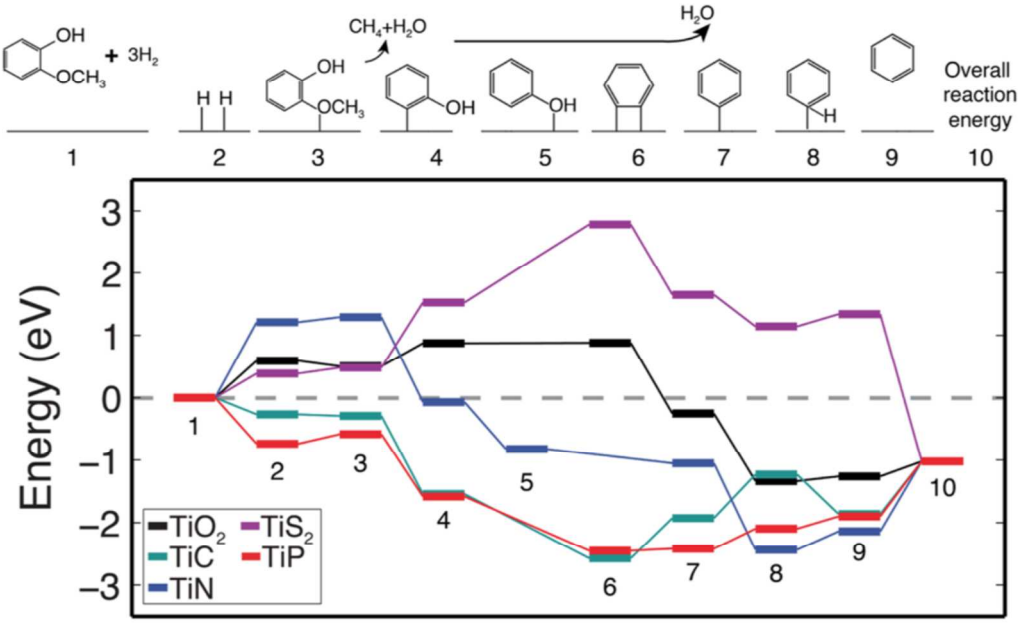


**Fig. 13** Thermodynamics of guaiacol deoxygenation over 5 Ti ceramic surfaces. Reprinted from Laursen *et al.*[73] with permission. Copyright 2017 American Chemical Society.

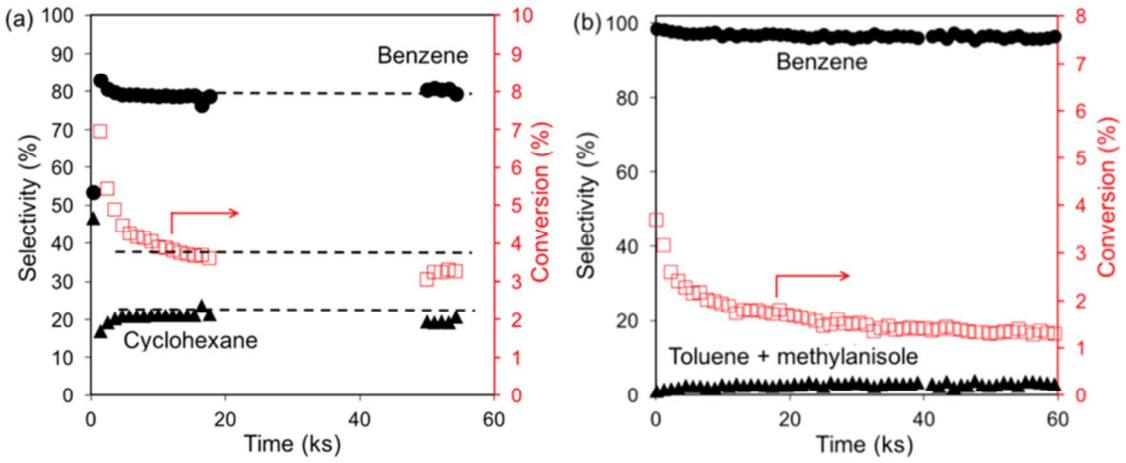


**Fig. 14** (a) Conversion and product selectivity for anisole HDO over mesoporous $Mo_2C$ catalyst. Conditions: feed, anisole (0.16%)/ $H_2$ (balance) (mol %) at ~110 kPa total pressure and at 423 K; total flow rate, ~1.67 $cm^3$ $s^{-1}$. (b) Conversion and product selectivity for anisole HDO over mesoporous $W_2C$ catalyst. Conditions: feed, anisole (0.06%)/ $H_2$ (balance) (mol %) at ~131 kPa total pressure and at 444 K; total flow rate, ~3.33 $cm^3$ $s^{-1}$. Reprinted from Lu *et al.*[25] with permission. Copyright 2016 American Chemical Society.